Concentration Dependent Chromatin States Induced by the Bicoid Morphogen Gradient

Colleen E. Hannon[1], Shelby A. Blythe[1] and Eric F. Wieschaus[1*]

[1]Department of Molecular Biology/Howard Hughes Medical Institute, Princeton University, Princeton, NJ 08544, USA

*Correspondence: efw@princeton.edu

ABSTRACT

In *Drosophila*, graded expression of the maternal transcription factor Bicoid (Bcd) provides positional information to activate target genes at different positions along the anterior-posterior axis. We have measured the genome-wide binding profile of Bcd using ChIP-seq in embryos expressing single, uniform levels of Bcd protein, and grouped Bcd-bound targets into four classes based on occupancy at different concentrations. By measuring the biochemical affinity of target enhancers in these classes *in vitro* and genome-wide chromatin accessibility by ATAC-seq, we found that the occupancy of target sequences by Bcd is not primarily determined by Bcd binding sites, but by chromatin context. Bcd drives an open chromatin state at a subset its targets. Our data support a model where Bcd influences chromatin structure to gain access to concentration-sensitive targets at high concentrations, while concentration-insensitive targets are found in more accessible chromatin and are bound at low concentrations.

INTRODUCTION

During embryonic development, multicellular organisms must generate the patterned tissues of an adult organism from a single undifferentiated cell. This process

requires highly regulated control of gene expression, both in developmental time and at reproducible positions in an embryo. These complex gene regulatory networks are controlled by systems of transcription factors, which bind to DNA and control the expression of genes required for development (Levine and Davidson, 2005). In early *Drosophila melanogaster* embryos, the Bicoid transcription factor forms an anterior-to-posterior protein gradient the embryo (Driever and Nüsslein-Volhard, 1988b). Bcd functions as transcriptional activator to pattern the embryo, binding to target gene enhancers and activating gene expression at distinct positions along the AP axis, corresponding to different concentrations of Bcd protein (Driever and Nüsslein-Volhard, 1988a; Struhl et al., 1989).

Recent studies of Bcd function suggest that its interaction with its targets may be more complex than the simple concentration-dependent activation originally proposed for morphogen gradients (Wolpert, 1969). In the absence of a strong Bcd gradient, embryos still exhibit patterned expression of Bcd target genes, and these genes can be activated at lower concentrations of Bcd than these nuclei would be exposed to in a wild-type embryo (Chen et al., 2012; Liu et al., 2013; Ochoa-Espinosa et al., 2009). While changing Bcd dosage shifts cell fates, the shifts deviate quantitatively from those expected of strict concentration dependence, especially as expression patterns are assayed progressively later during development (Liu et al., 2013). These studies have consequently raised doubts about the extent to which the local concentration of Bcd along its gradient determines the spatial patterns of target gene expression in the embryo.

While these studies argue against a strict application of the morphogen hypothesis for Bcd, the patterned expression of target genes is also influenced by other maternal patterning systems and interactions among the Bcd targets themselves (Chen et al., 2012; Jaeger, 2010; Löhr et al., 2009). Chen, *et al*. have shown that the posterior boundaries of Bcd target genes are positioned by a system of repressors including Runt, Krüppel, and Capicua. This work suggests that the Bcd gradient does not directly establish expression domains of its target genes but rather is just one player in a network of patterning genes that influence cell fates in the embryo. However, using target gene expression as a metric for Bcd function does not address how information from the Bcd gradient initially establishes distinct cell fates.

Part of the difficulty in evaluating direct roles of the Bcd gradient arises from the unknown nature of the molecular mechanism by which Bcd establishes concentration thresholds different positions along the gradient. A simple model of the positioning of Bcd target genes predicts that *cis*-regulatory elements of different genes respond to different concentrations of Bcd. Genes in the anterior would have low affinity Bcd binding sites and could therefore only be activated by high Bcd concentrations, whereas genes expressed in more posterior positions would have higher affinity binding sites (Driever et al., 1989b). Direct measurements of Bcd binding affinity have been conducted *in vitro* using DNA probes (Burz et al., 1998; Gao and Finkelstein, 1998; Ma, 1996; Ma et al., 1996) and have demonstrated that Bcd is able to bind cooperatively to achieve sharp concentration thresholds. While these measurements lend some support to a simple affinity model, little correlation has been shown between predicted binding site affinity and AP position of gene expression (Ochoa-Espinosa et al., 2005; Segal et

al., 2008). However, neither *in vitro* measurements of Bcd binding nor computational predictions of binding sites can capture interactions between Bcd and its target enhancers in the context of local chromatin structure.

Using high throughput sequencing approaches, we measured *in vivo* genome-wide Bcd-DNA binding and chromatin accessibility in transgenic embryos expressing different concentrations of uniform Bcd protein. These data reveal distinct classes of enhancers that differ in their sensitivity to Bcd concentration. We find that these classes differ both in the DNA binding motifs that they contain and in their local chromatin accessibility. We also find that Bcd influences the accessibility of a subset of its target enhancers, primarily at highly concentration-sensitive enhancers that drive gene expression in the anterior of the embryo. This leads us to a model in which target enhancers throughout the genome have a broad range of sensitivities for Bcd protein, and can therefore respond to a range of Bcd concentrations along the gradient. However, rather than arising from differences in Bcd binding site composition, these *in vivo* interactions are chromatin context-dependent, and Bcd influences the chromatin structure of its target enhancers.

RESULTS

Bicoid target gene expression boundaries are influenced by other maternal factors, but its physical interaction with enhancers is not

To investigate the mechanism whereby Bcd functions to pattern the AP axis, we performed chromatin immunoprecipitation followed by high throughput sequencing (ChIP-seq) to determine the genome-wide binding profile of Bcd to its targets. We performed the ChIP-seq experiments on embryos expressing GFP-tagged Bcd in a *bcd*

null mutant background that were staged precisely in nuclear cycle 14 (NC14), and established a list of robust and reproducible list of 1,027 peak Bcd binding regions (see Supplemental File 1 and Experimental Procedures). These peaks successfully identify 63 out of 66 of the previously identified Bcd target enhancers (Chen et al., 2012) and overall associate with enhancers whose expression patterns span broadly across the AP axis.

As a transcriptional regulator, Bcd activates the expression of a subset of its targets whose expression domains are predominantly located in the anterior half of the embryo. In *bcd* mutant embryos, such targets are not expressed. For example, the gap genes *buttonhead* (*btd*) and *knirps* (*kni*) have anterior expression domains that are not present in *bcd* mutant embryos (Figure 1A). The posterior *kni* expression domain, however, is expressed in *bcd* embryos, albeit with shifted positional boundaries. These distinct domains of *kni* expression are controlled by separate enhancer elements (Pankratz et al., 1992; Schroeder et al., 2004), both of which are bound by Bcd *in vivo* (Supplemental File 1). In the absence of all maternal AP patterning inputs (*bicoid nanos hunchback torsolike* quadruple mutants), the *kni* posterior enhancer is not expressed. However, in embryos where Bcd is the sole source of maternal patterning information (*nanos hunchback torsolike* triple mutants), the *kni* posterior domain is expressed with a near wild-type anterior expression boundary (Figure 1A and Figure 1 Figure Supplement 1A). The *kni* posterior domain therefore represents a second class of Bcd target gene, which depends on Bcd to determine the position of its expression but does not demonstrate an absolute requirement of Bcd for transcriptional activation.

Both classes of Bcd target genes receive positional cues both from Bcd and from other patterning systems. We considered the possibility that, given their influence on the expression domains of Bcd target genes, the posterior and terminal patterning systems may impact Bcd binding to its target enhancers in different nuclei along the AP axis. We therefore tested whether loss of the posterior and terminal systems (*nanos* and *torsolike*) would alter the Bcd ChIP-seq profile. We used the statistical package EdgeR (Robinson et al., 2010) to test for differential Bcd binding between wild-type and *nanos torsolike* embryos and found that we could not detect any significant change in binding at any of these 1,027 regions (Figure 1 Figure Supplement 1B). Therefore, although the expression domains of Bcd target genes are ultimately influenced by inputs from other AP patterning systems, the physical interaction of Bcd with the DNA in the enhancers of these genes occurs independently of other maternal AP patterning inputs.

Embryos expressing Bcd uniformly show developmental fates reflecting the concentration of Bcd

We set out test whether incremental changes in Bcd concentration along the gradient can be read out directly at the level of binding to target enhancers. Due to the graded distribution of Bcd, each nucleus along the AP axis is exposed to a different concentration of the protein. To measure the Bcd binding state at individual concentrations, we performed ChIP-seq on embryos expressing Bcd at single, uniform concentrations in every nucleus along the AP axis. Several previous studies have included genetic manipulations in which the Bcd gradient has been flattened to assess its activity independently of its distribution (Chen et al., 2012; Driever and Nüsslein-Volhard, 1988a; Löhr et al., 2009; Ochoa-Espinosa et al., 2009). However, genetically

disrupting the gradient does not result in a total flattening, and transgenic approaches to date have not allowed for precise and reproducible control over the level of expression of the flattened Bcd. We therefore generated transgenic lines expressing GFP tagged Bcd in which the endogenous 3'UTR responsible for graded localization is flanked by FRT sites that allow it to be replaced with the unlocalized *spaghetti squash* 3'UTR. To generate different expression levels of uniform Bcd, we coupled transgenes to different maternally active promoters that yield embryos in which individual uniform Bcd concentration approximates single positions along the gradient (see Figure 1 Figure Supplement 1C).

To determine the expression levels of the uniform lines, we imaged GFP fluorescence in live embryos expressing either uniform or graded GFP-Bcd (Gregor et al., 2007a) (Figure 1B). The endogenous *bcd* promoter drives a level of uniformly expressed Bcd equivalent to that measured at approximately 65% egg length of the wild-type gradient. The *matrimony (mtrm)* and *αTubulin67C (αTub67C)* promoters drive expression levels corresponding to approximately 45% and 25% egg length, respectively. For simplicity, we refer to the uniform lines as low (*bcd* promoter), medium (*mtrm* promoter), and high (*αTub67C* promoter). (See also Figure 1 Figure Supplement 1D)

Uniform expression of Bcd confers gene expression profiles and developmental programs representative of distinct positions along the AP axis. The head gap gene *buttonhead (btd)* is expressed in an anterior stripe in wild-type embryos (Figure 1A), but expands to fill the entire middle of the embryo at the highest level of uniform Bcd (Figure 1C). At the medium level, the Btd anterior stripe is duplicated at the posterior, and at the

lowest Bcd level, it is not expressed. The gap gene *knirps*, which is expressed in an anterior domain and a posterior stripe, shows a duplication of its anterior domain in the posterior in high uniform Bcd embryos. There is also a weaker duplication at the medium Bcd level. There is no apparent anterior expression at the lowest level, but an expanded posterior stripe is present. The gene expression patterning we observe in the presence of uniform Bcd likely result from the activity of additional maternal patterning cues (*nanos* and *torso*) as well as interactions between the Bcd target genes themselves. The concentration-dependent activity of uniform Bcd is also apparent in cuticle preparations of embryos expressing the transgenic constructs. The transgenic constructs specify increasingly anterior structures along larval body plan as the concentration of Bcd increases (Figure 1D). These effects on the body plan indicate that the uniform Bcd transgenes are capable of specifying cell fates that reflect their relative expression levels.

Bcd binding to genomic targets is concentration dependent

We next determined genome-wide Bcd binding profiles at each individual concentration by ChIP-seq and used these measurements to assign each of the 1,027 peak regions to classes distinguished by their degree of concentration-dependent Bcd binding (Figure 2A). Using EdgeR (Robinson et al., 2010), we selected peak regions that exhibited statistically significant (FDR ≤ 0.05) differences in binding by performing pairwise exact tests between the three uniform Bcd concentrations. This yielded four different classes of peaks, one concentration-insensitive class, and three classes with increasing sensitivity to Bcd concentration.

The Concentration-Insensitive peak class (n = 143) shows no significant differences between any of the concentrations of uniform Bcd we tested. Concentration-Sensitive III peaks (n = 593) are significantly reduced in binding between the highest and lowest Bcd concentrations, but reductions are not significant between high and medium, or medium and low. Concentration-Sensitive II peaks (n = 138) are significantly reduced in binding at the lowest Bcd level compared to either the medium or the high levels. Finally, Concentration-Sensitive I peaks (n = 152) are significantly reduced in binding at both the medium and the low Bcd levels compared to the highest level (Figure 2A). These different groups suggest that Bcd binds differentially to target enhancers at specific concentrations, and furthermore that certain subsets of enhancers are bound only in anterior nuclei whereas others are bound broadly across the entire AP axis.

Although 63 out of 66 previously characterized Bcd-dependent enhancers are identified in our ChIP peaks, the majority of the 1,027 peaks identified have not been extensively examined. Within the set of known Bcd targets, there is strong correlation between position of expression and the associated Bcd sensitivity class (Figure 2A). To extend this observation to previously uncharacterized Bcd target enhancers, we queried the Fly Enhancer resource generated from the Vienna Tile GAL4 reporter library (Kvon et al., 2014). The Fly Enhancer collection is a library of candidate enhancer DNA fragments driving expression of GAL4 that covers 13.5% of the non-coding genome. Each fragment's expression pattern has been measured and scored by developmental stage. A total of 293 enhancer candidates overlap with at least one peak in our data set. Of these, 163 drive gene expression in stage 4-6 (which includes NC14), and these

active enhancers overlap with a total of 151 (14.7%) of the Bcd-peaks. The remaining overlapping fragments either are active later in development (75), or are not functional (55). Given the large fraction of the queried enhancers that are active during early development (163 out of 293 overlapping enhancers), it remains possible that a similar fraction of the of the 876 peaks (77.2%) that do not overlap with the Fly Enhancer candidates may correspond to enhancers active in the early embryo.

The Bcd sensitivity classes are predictive of the expression domains of associated enhancer fragments. Enhancers overlapping with both the Concentration-Sensitive I and II classes drive expression in anterior regions of the embryo, with the Concentration-Sensitive III and Concentration-Insensitive classes driving broad and posterior expression, respectively (Figure 2B). This indicates that our classifications of the Bcd-bound peaks reflect unique groups of Bcd targets with differing abilities to bind Bcd protein and consequently activate gene expression in different positions along the AP axis. The boundary positions of anteriorly expressed Bcd targets may be refined at the transcriptional level by interactions with opposing gradients of repressors like Runt (Chen et al., 2012), that are Bicoid targets themselves. We addressed whether such repression could account for the restricted expression of Concentration-Sensitive I and II targets to anterior regions of the embryo by examining whether they were enriched for binding of such repressors. By comparison with genome-wide binding profiles of transcription factors in the BDTNP ChIP database (Li et al., 2008; MacArthur et al., 2009), we instead find that the factors associated with each Bcd peak class are generally those whose expression patterns overlap with the average expression domains of each class (Figure 2 Figure Supplement 1A). Peaks in the Concentration-

Sensitive I class, for example, are enriched for binding of the terminal gap gene Huckebein whereas those in the Concentration-Sensitive II class are enriched for Krüppel and Giant binding. However, we find no evidence that the Bcd sensitivity classes are predominantly defined by repressive interactions.

Sequence composition of ChIP sensitivity classes does not account for *in vivo* sensitivity to Bcd concentration

We next wanted to determine whether the Bcd-bound regions in each sensitivity class differ at the level of DNA sequence. *In vitro,* Bcd binds with high affinity to the consensus 5'-TCTAATCCC-3', and that variations on this consensus sequence constitute weak binding sites (Burz et al., 1998; Driever and Nüsslein-Volhard, 1989; Driever et al., 1989b). If the affinity of a given enhancer for Bcd were encoded primarily at the level of its DNA sequence, we would expect to see a higher representation of strong Bcd binding sites in the less sensitive classes, and weaker sites in the more sensitive classes. To test this, we performed *de novo* motif discovery using the RSAT peak-motifs algorithm (Thomas-Chollier et al., 2012; 2008). We identified the top motifs in the entire Bcd ChIP peak list, ranked by their e-value, and found that the top three most highly ranked motifs were the consensus binding site for the proposed pioneer factor Zelda (Zld) (Bosch et al., 2006; De Renzis et al., 2007; Harrison et al., 2011; Nien et al., 2011), and a strong (TAATCC) and weak (TAAGCC) Bcd binding site (Figure 2C). We next calculated the frequency with which these motifs appear in each peak, and tested for enrichment between sensitivity classes by permutation test (Figure 2D). We found that despite their failure to bind Bcd at low concentrations, the Concentration-Sensitive I and II classes are enriched for both the strong and weak Bcd sites relative to

the peak set as a whole. Given our result that these classes drive expression primarily in the anterior of the embryo (Figure 2B), the higher density of Bcd binding sites in these enhancers contrasts with previous studies that have found little correlation between number of binding sites and position of gene expression (Ochoa-Espinosa et al., 2005). This difference likely reflects the larger sample size used in our study, as well as our method for classifying Bcd bound peaks. The Concentration-Sensitive III class did not contain an enrichment of any site over the total peak set. The Concentration-Insensitive class, however, showed a higher prevalence of the Zld binding site relative to the total peak set than any other class.

These results indicate that, in contrast to a binding site affinity model for Bcd function, Bcd target enhancers that behave as concentration-sensitive and -insensitive *in vivo* are not distinguished by their representation of strong versus weak Bcd binding sites, confirming previous studies (Ochoa-Espinosa et al., 2005). In further support of this concept, we found little correlation between *in vitro* binding affinity by electrophoretic mobility shift assay and the *in vivo* binding properties we observe by ChIP for a selected subset of peaks (Figure 2 Figure Supplement 2). At the level of sequence composition, they instead appear to differ in their balance of Bcd and Zld binding sites. Although both strong and weak Bcd sites and Zld sites are enriched in the Bcd ChIP peaks as a whole, there is a bias toward both Bcd sites in peaks that show concentration-sensitive binding properties by ChIP-seq and a bias toward Zld sites in the concentration-insensitive peaks. Zld, a ubiquitously expressed early embryonic transcription factor, has been implicated in chromatin remodeling prior to zygotic genome activation (Harrison et al., 2011; Nien et al., 2011; Sun et al., 2015). The

predominance of Zld motifs over Bcd motifs in the Concentration-Insensitive class suggests that *in vivo* chromatin structure also plays a role in the sensitivity of a given target to transcription factor concentration in the context of the developing embryo. Taken together, these findings suggest that the chromatin context of an enhancer may play a greater role in its overall affinity for a transcription factor *in vivo* than the sequences of the binding sites that it contains. We therefore set out to test the hypothesis that sensitivity classes are distinguished at the level of chromatin structure.

Bcd is required for chromatin accessibility at a subset of concentration-sensitive target sites

To measure genome-wide patterns of chromatin accessibility and nucleosome positioning, we performed ATAC-seq (Buenrostro et al., 2015) on single wild-type embryos precisely staged at 12 minutes after the onset of NC14, and identified 13,266 peaks of chromatin accessibility (see Experimental Procedures). Of the 1,027 Bcd-bound regions identified by ChIP-seq, 855 (83.3%) of them overlap with ATAC-seq peaks.

Given Zelda's role in influencing chromatin accessibility and the presence of its binding sites at Bcd-bound regions of genome, we measured the effect of Zld on accessibility at Bcd sites by ATAC seq (Figure 3A). Of the total 13,226 accessible regions at NC14, 2,675 (20.2%) show a significant reduction in accessibility in *zld* mutant embryos. This fraction is higher in Bcd-bound peaks; 402 (39.1%; or 379 [44.3%] of 855 the Bcd peaks that overlap with ATAC open regions, see Table S5) show reduced accessibility in *zld* mutants, indicating that Bcd bound regions are more likely to be dependent on Zld for their accessibility than the genome as a whole.

297 However, the Zld-dependent peaks are distributed across each sensitivity class
298 determined by ChIP, with no particular class being significantly more Zld-dependent.
299 This contrasts with the distribution of binding sites in the peak classes, which revealed
300 that the Concentration-Insensitive peaks were more likely to contain Zld binding sites.
301 These results suggest that while Zld contributes to the accessibility of a subset of Bcd
302 target gene enhancers, it is unlikely to determine the differential concentration sensitivity
303 of Bcd peaks as a whole.

304 Given the enrichment for both strong and weak Bcd binding sites in the
305 Concentration-Sensitive I and II classes, we next examined the impact of Bcd protein
306 itself on chromatin accessibility by ATAC seq (Figure 3A). In *bcd* mutants, 326 (2.4%) of
307 the 13,266 open regions in wild-type embryos show significantly reduced accessibility
308 accompanied by increased nucleosome occupancy in those same regions (Figure 3A
309 and B). These regions are therefore either directly or indirectly dependent on Bcd for
310 their accessibility. More strikingly, 132 (12.9%) of the 1,027 Bcd ChIP-seq peaks show
311 reduced accessibility in the absence of Bcd and likely represent regions where Bcd's
312 impact is direct. These regions dependent on Bcd for accessibility are significantly
313 enriched for peaks in the Concentration-Sensitive I and II classes (32.9% and 31.9% of
314 each class, with Fisher's exact test P-values of 4.29×10^{-12} and 1.37×10^{-10}, respectively).
315 In contrast, the Concentration-Sensitive II and Concentration-Insensitive classes are
316 both significantly underrepresented (6.07% and 0.7% and P-values = 7.88×10^{-13} and
317 2.29×10^{-8}) (Figure 3B). This suggests that Bcd binding influences chromatin
318 accessibility preferentially at a subset of highly concentration-sensitive enhancers.

Because the Concentration-Sensitive I and II classes are bound primarily at high Bcd concentrations, Bcd's effects on chromatin accessibility at these targets likely occurs only in anterior regions of the embryo. In support of this, we find that chromatin accessibility at Bcd-dependent, concentration-sensitive targets is responsive to Bcd concentration. Expressing uniform Bcd confers accessibility to peaks that are not accessible in *bcd* mutant embryos (Figure 3B). The degree of chromatin accessibility conferred by Bcd correlates positively with the concentration of uniform Bcd expressed (Figure 3B). This observation, along with the overrepresentation of the Concentration-Sensitive I and II classes in the Bcd-dependent peaks, suggests that Bcd influences the chromatin state of these targets primarily at the high concentrations found in the anterior of the embryo.

A second feature that distinguishes the chromatin structure of Bcd binding sites is the presence of DNA sequences favorable for nucleosome occupancy (Segal et al., 2006). Bcd bound regions in wild type embryos are generally depleted of nucleosomes (Figure 4A). However, predicting nucleosome positioning sequences using the NuPoP algorithm (Xi et al., 2010) suggests that the Concentration-Sensitive I and II Bcd enhancer classes are more likely to bind nucleosomes than the Concentration-Sensitive III and Concentration-Insensitive classes. (Figure 4B). The contrast between predicted occupancy and observed depletion suggests that these regions are actively restructured for Bcd and other transcription factors to bind. The increased nucleosome preference of the more Concentration-Sensitive peaks, combined with the observation that these sites become occupied by nucleosomes in *bcd* mutants suggests a model where Bcd, either directly or in combination with cofactors is able to direct chromatin remodeling events,

which may play a significant role in distinguishing concentration-sensitive and -insensitive targets. Additionally, we find that Bcd-bound regions that are dependent on either Zld or Bcd for their accessibility are more likely to have a higher nucleosome preference than regions that are independent of both factors (Figure 4C). This further suggests that Bcd is able to overcome a high nucleosome barrier in a manner similar to Zld (Sun et al., 2015) at a subset of its target enhancers.

These effects of chromatin accessibility impact the availability of sequence motifs for binding Bcd. In wild type embryos, there is a gradual increase in average motif accessibility from high to low sensitivity, and this difference becomes more pronounced in *bcd* mutant embryos (Figure 4D), consistent with a role for Bcd in driving changes in accessibility at more sensitive sites in a concentration dependent manner. This is also evident at the level of nucleosome organization. Calculating the fraction of motifs that overlap nucleosomes in either wild type or *bcd* mutant chromatin conformations, we find that whereas on average across all sensitivity classes 55 ± 2% of Bcd motifs are in nucleosome-free tracts in wild-type embryos, in *bcd* mutant embryos motifs have lower overall accessibility and a graded association with nucleosomes that correlates with the sensitivity classes (41%, 46%, 50%, and 53% of motifs are accessible from high to low sensitivity). These results indicate that the mechanistic determinants of concentration-dependent Bcd action likely involve a complex interaction between Bcd, DNA, and chromatin structure.

A truncated Bcd protein shows reduced binding specifically at concentration-sensitive target enhancers

364 A chromatin remodeling activity associated with Bcd has not been previously
365 described. We hypothesize that Bcd renders its target sites accessible either by
366 competing with nucleosomes to access its binding sites and bind to DNA at high
367 concentrations or by recruiting chromatin-remodeling enzymes to accessible motifs and
368 subsequently driving local nucleosome remodeling to render more sites accessible. We
369 reasoned that if Bcd can displace nucleosomes simply by competing with them for
370 access to its binding sites, it should be possible for the Bcd DNA-binding homeodomain
371 to compete. However, if Bcd instead drives remodeling via recruitment of cofactors, it is
372 likely that these interactions or activities are carried out through regions of the protein
373 outside of the DNA binding domain. To distinguish between these two possibilities, we
374 designed a transgenic GFP-Bcd construct that is truncated downstream of the
375 homeodomain. We modeled the truncated Bcd protein after the *bcd*^{085} allele, which was
376 originally classified as an "intermediate allele" of *bcd* (Frohnhöfer and Nüsslein-Volhard,
377 1986) and reported to have weak transcriptional activating activity (Struhl et al., 1989).
378 The truncation occurs 28 amino acids downstream of the homeodomain (Figure 5A),
379 and the GFP-tagged protein was therefore expected to bind DNA but lack functions
380 requiring its C-terminus. The truncated protein (known as GFP-Bcd^{085}) forms a gradient
381 from the anterior of the embryo, and is expressed at a similar level as a full-length GFP-
382 Bcd (Figure 5B).
383 By ChIP-seq, we found that compared to wild-type, GFP-Bcd^{085} binding in the
384 Concentration-Sensitive I and II enhancer classes was significantly reduced relative to
385 the Concentration-Sensitive II and Concentraiton-Insensitive classes (p-value < 0.0001
386 in permutation test with n = 10,000 trials) (Figure 5C). Our ATAC-seq experiments

revealed that these classes have reduced chromatin accessibility in *bcd* mutants (Figures 3B and 4D). Taken together, these results suggest that Bcd's ability to access its concentration-sensitive targets is dependent upon activities carried out by domains in the C-terminus of the protein, likely via recruitment of a cofactor, and that its DNA binding activity alone is insufficient to drive chromatin accessibility.

Bicoid binding sites confer anterior expression to a posterior target

Overall, highly concentration-dependent targets are expressed in the anterior and are dependent on Bcd for accessibility, while less sensitive targets show more posterior expression patterns and a greater enrichment for Zld binding sites. An enhancer for *caudal* is a Concentration-Insensitive Bcd target and drives expression in the posterior of the embryo (Figure 6). This enhancer depends on Zld for chromatin accessibility, and consequently is not functional in *zld* mutants (Supplemental File 1 and Figure 6B). This supports previous findings that Zld binding contributes to allowing Bcd activation at low concentrations in posterior nuclei (Xu et al., 2014). Like the *kni* posterior enhancer (Figure 1A), the *caudal* enhancer is Bcd independent for chromatin accessibility and its expression boundary shifts anteriorly in *bcd* mutant embryos. We tested whether we could convert the properties of the *caudal* enhancer from low to high sensitivity by manipulating DNA motifs. We identified the Zld binding sites in the *caudal* enhancer sequence and mutated them to Bcd binding sites (Figure 6A). These mutations result in a shift of *caudal* reporter expression to the anterior of the embryo. Anterior expression of the mutated reporter is Bcd dependent, as it is lost in *bcd* mutant embryos. Importantly, the mutant enhancer is functional in *zld* mutant embryos, retaining a distinct anterior expression domain. In the absence of Zld, the wild type enhancer does not

drive expression. (Figure 6B) By replacing Zld motifs with Bcd motifs, the enhancer retains functionality, but the spatial domains of expression are now restricted to regions of high Bcd concentration. These results are consistent with a model where Bcd operates at high concentrations to confer chromatin accessibility at target sites, thereby delineating distinct gene expression and chromatin states at specific positions along its concentration gradient.

DISCUSSION

A model for chromatin accessibility thresholds at Bcd target genes

The results presented here demonstrate that the positional information in the Bcd gradient is read out as differential binding between Bcd and the *cis*-regulatory regions of its target genes. The overrepresentation of enhancers for anteriorly expressed target genes in the more sensitive classes provides support for the classic French flag model, as their enhancers are only capable of binding Bcd at high levels. However, motif analysis and *in vitro* EMSA experiments reveal that the differences in binding affinities that we observe *in vivo* cannot be explained entirely by the sequence of Bcd binding sites in the target enhancers. Instead we find that a subset of the enhancers in the concentration-sensitive classes require Bcd for chromatin accessibility. Taken together, this leads us to model in which the Bcd morphogen establishes concentration thresholds along the AP axis of the developing embryo by driving opening chromatin states at high concentrations, thereby gaining access to its most sensitive target enhancers. At lower concentrations in more posterior nuclei, Bcd is unable to access these enhancers, and therefore does not bind and activate their transcription. (Figure 7) In this way, expression of these concentration-sensitive target genes is restricted to

anterior regions of the embryo. The higher density of Bcd binding sites in highly concentration-sensitive target enhancers (shown in Figure 2B) suggests that these enhancers may require a larger number of Bcd molecules to be bound at a given time to keep the enhancers free of nucleosomes and accessible to the additional regulatory factors. We therefore provide a model for morphogen function in which the concentration thresholds in the gradient are read out molecularly at the level of chromatin accessibility, rather than through the strength of binding sites in the target enhancers.

It is important to note that the discrete sensitivity classes described here were generated by Bcd binding data, and this binding occurs prior to the activation of target genes and refinement of their expression domains. In our model Bcd establishes these initial patterns not by competing with its own target genes, but with default nucleosome positions in the early embryo. We predict that this initial interaction with chromatin is an essential event for establishing distinct, positionally defined patterns of gene expression. The chromatin landscapes established early by Bcd are then elaborated upon by additional patterning factors, including Bcd target genes themselves, as well as the repressor gradients proposed by Chen, *et al.* (Chen et al., 2012) Thus, the pre-transcriptional information presented by Bcd in the form of differential binding states is refined at the level of gene expression domains both by Bcd and other transcription factors active in the early embryo.

Relationship of Bicoid and Zelda at Bicoid-bound enhancers

The prominence of the Zld binding motif in the Bcd-bound ChIP peaks and ATAC-seq in *zld* mutants reveals that Zld also contributes to the accessibility of Bcd

456 targets in the genome, in part at those targets that are not dependent on Bcd for their
457 accessibility (61/1,027 peaks are dependent on both Bcd and Zld for accessibility). Zld
458 is therefore likely to be one component that influences the accessibility and therefore
459 the apparent *in vivo* affinity of the enhancers that are bound by Bcd but insensitive to its
460 local concentration (Figure 7). Previous work has suggested that Zld contributes to
461 activation of target genes at low concentrations of Bcd protein (Xu et al., 2014). That
462 study, in combination with the work presented here, allows us to predict that
463 transforming a concentration-sensitive Bcd target enhancer into a Zld dependent
464 enhancer would increase the accessibility and therefore the sensitivity of that region *in*
465 *vivo.* Indeed, Xu, *et al.* have previously demonstrated that adding increasing numbers of
466 Zld sites to an inactive Bcd-bound enhancer can drive increasingly posterior gene
467 expression (Xu et al., 2014). The reporter construct used to demonstrate this effect
468 (HC_45) is identified as a Concentration-Sensitive I target in our study. We posit that
469 the increase in gene expression from this reporter observed in their work is the result of
470 increasing the accessibility of the enhancer region.
471 Alternately, when we replace Zld sites with Bcd sites in an enhancer that drives
472 posterior expression, the expression domain shifts to the anterior of the embryo. This
473 demonstrates that without Zld to keep the enhancer open in posterior nuclei, activation
474 of the reporter gene becomes entirely dependent on Bcd, effectively shifting this
475 reporter from a concentration-insensitive to concentration-sensitive enhancer. This
476 finding fits with both previously reported findings and the model proposed in our study.
477 Namely, that Zld contributes to the accessibility of Bcd target genes throughout the

478 embryo, while high levels of Bcd can drive accessibility independently and activate gene
479 expression at a subset of targets in the anterior of the embryo.
480 The reduced binding by a truncated Bcd protein at the most concentration-
481 sensitive targets indicates that Bcd does not displace nucleosomes by simply by
482 competing for binding to genomic targets, but rather that the C-terminus of the Bcd
483 protein is required for accessing its nucleosome-associated DNA targets. Previous work
484 has shown that various domains of the Bcd protein are required for interactions with
485 both co-activators and co-repressors. The N-terminus of Bcd is required for interactions
486 with components of the Sin3A/HDAC repressor complex, and these interactions are
487 proposed to play a role in reducing Bcd's transcriptional activation activity (Zhao et al.,
488 2003; Zhu et al., 2001). Multiple Bcd domains, including the C-terminus, are required for
489 interaction with CREB-binding protein (CBP), which has histone acetyltransferase
490 activity (Fu and Ma, 2005; Fu et al., 2004). It is possible that in our truncated Bcd
491 construct, this interaction with CBP is disrupted. As CBP is thought to play a role in
492 increasing chromatin accessibility for transcription factors (Chan and La Thangue,
493 2001), the loss of this interaction could lead to the reduced binding to sensitive targets
494 that we observe in embryos with truncated Bcd. The enhancers that we have classified
495 as concentration-insensitive do not depend on Bcd to establish an open chromatin
496 state. This suggests that these sites are opened by other chromatin remodeling factors,
497 or are inherently more likely to be nucleosome-free based on their underlying sequence.
498 It has previously been suggested that transcription factors can compete with
499 nucleosomes for access to their DNA binding sites (Mirny, 2010; Wang et al., 2011).
500 This could occur through cooperative binding to nucleosome-associated enhancers: if

one Bcd molecule could gain access to a binding site that was protected by a nucleosome, it could recruit additional Bcd protein molecules to bind to nearby sites and occlude nucleosome binding. This cooperativity would require a high concentration of Bcd protein, fitting with our observation that Bcd influences accessibility more strongly at high concentrations. However, our experiments with a truncated Bcd protein reveal that Bcd cannot bind to its most sensitive targets without its C-terminal domains. As many of the residues that have been implicated in cooperative binding reside in the Bcd homeodomain (Burz and Hanes, 2001), we would expect this truncated Bcd to bind cooperatively. This finding therefore supports a model in which Bcd is actively remodeling chromatin, either directly or more likely by interacting with chromatin remodeling factors through its C-terminus.

As a maternally supplied factor, Bcd provides one of the first cues to the break the symmetry of the embryonic body plan. Our results suggest that this symmetry breaking occurs first at the level of chromatin accessibility, as Bcd drives the opening of its most concentration-sensitive target enhancers in anterior nuclei. Another maternal factor, Zld, is proposed to act as a pioneer factor at early embryonic enhancers with a high intrinsic nucleosome barrier. By binding to these enhancers, Zld depletes them of nucleosomes and allows patterning transcription factors to bind and activate gene expression (Sun et al., 2015). We have demonstrated here that Bcd influences the accessibility primarily of its concentration-sensitive targets, which also exhibit a high predicted nucleosome barrier (Figure 4B). This raises the possibility that Bcd may be exhibiting pioneer-like activity at high concentrations, driving accessibility of these sites prior to transcriptional activation. It is unlikely that Bcd is unique in its ability to influence

524 the local chromatin accessibility of its targets. Recent work in mouse embryos has
525 shown that another homeodomain transcription factor, Cdx2, influences the chromatin
526 accessibility of its targets during posterior axial elongation (Amin et al., 2016). This may
527 be a common property of developmental transcription factors that must gain early
528 access their target enhancers while the chromatin state of the genome is being
529 remodeled during large-scale transitions in the gene regulatory landscape.
530

531 **EXPERIMENTAL PROCEDURES**

532 **Fly stocks and Genetics**

533 *bcd* mutants refers to embryos derived from bcd^{E1} homozygous mothers. The bcd^{E1} and
534 bcd^{E1} nos^{L7} tsl^{4} stocks were from the Wieschaus/Schüpbach stock collection maintained
535 at Princeton University. *zld* mutants are embryos derived from $zelda^{294}$ germline clones.
536 Zelda mutant embryos were generated from the zld^{294} allele (kind gift of Christine
537 Rushlow) as germline clones as described previously (Blythe and Wieschaus, 2015).
538 Uniform Bcd and Bcd^{085} transgenes were expressed in a bcd^{E1} mutant background.
539 Germline clones possessing only positional information from Bicoid were generated by
540 heat shocking *hsFLP; FRT82B* hb^{FB} nos^{BN} tsl^{4}*/ FRT82B* tsl^{4} Ovo^{D} larvae. Germline
541 clones lacking Bicoid positional information as well were generated by heat shocking
542 *hsFLP; FRT82B* bcd^{E1} hb^{FB} nos^{BN} tsl^{4}*/ FRT82B* tsl^{4} Ovo^{D} larvae. Embryos from
543 homozygous *eGFP-Bcd;* bcd^{E1} nos^{L7} tsl^{4} mothers were used in ChIP-seq experiments to
544 determine the impact of removing other maternal factors on Bcd binding to its targets.
545 All ATAC-seq experiments were performed in a *His2Av-GFP* (Bloomington) background
546 to facilitate scoring of nuclear density.

The uBcd and Bcd^{085} constructs were injected for site directed transgenesis into embryos from a *y,w;attp40* stock by Genetic Services (bcd-uBcd and αTub67C-uBcd) or BestGene (mtrm-uBcd and Bcd^{085}) and stable transformant lines were established. The mutant cad-GAL4 reporter was injected into a *M{vas-int.Dm}ZH-2A, P{CaryP}attP2* stock by Rainbow Transgenic Flies, Inc.

The uBcd transformants expressed eGFP-tagged Bcd in a graded distribution in the embryo and RFP in the eyes. Transgenic flies containing the uBcd constructs were crossed into a bcd^{E1} background. To achieve uniform Bcd expression, the uBcd flies were crossed to a stock expressing a heat shock-inducible *flippase* in a bcd^{E1} background and the resulting larvae were heat shocked at 37°C. Recombination of the FRT-flanked cassette containing the *bcd* 3'UTR and 3xP3-RFP was scored by a mosaic loss of RFP expression in the eyes. Mosaic flies were further outcrossed to bcd^{E1} and progeny lacking the bcd 3'UTR were sorted by loss of RFP expression. The resulting flies produced embryos in which the bcd 3'UTR was replaced by the sqh 3'UTR causing a uniform distribution of Bcd along the AP axis. (Figure 1 Figure Supplement 1C)

Transgenic Constructs

The uniform Bcd constructs were generated using a pBABR plasmid containing an N-terminal GFP-tagged *bcd* cDNA in which the *bcd* 3'UTR was replaced by the *sqh* 3'UTR (pBABR GFP-Bcd3'sqh) (Oliver Grimm, unpublished). This results in a loss of mRNA localization at the anterior pole of the oocyte. A sequence containing the *bicoid* 3'UTR and a 3xP3-RFP reporter flanked by FRT sites was synthesized by GenScript and cloned by Gibson Assembly into the pBABR GFP-Bcd3'sqh plasmid. The FRT-flanked

cassette was inserted between the *bcd* coding sequence and the *sqh* 3'UTR. The *bcd* promoter was removed by digesting with AgeI and KpnI and replaced with either the *mtrm* or the *αTub67C* promoter to generate the *bcd-uBcd*, *mtrm-uBcd*, and *αTub67C-uBcd* constructs.

The GFP-Bcd^{085} truncation was generated from eGFP-Bcd (Gregor et al., 2007a) in pBlueScript by amplifying with primers to create a stop codon after amino acid 179 as in the *bcd^{085}* hypomorphic EMS allele (Rivera-Pomar et al., 1996). The primers inserted an *AvrII* restriction site 3' to the deletion site.

F Primer: 5'-TTGtagCCTAGGCCTGGATGAGAGGCGTGT-3'

R Primer: 5'-TCCAGGCCTAGGctaCAAGCTGGGGGGATC-3'

The plasmid was amplified by PCR and the linear product was digested and ligated to create the Bcd^{085} truncation. The GFP-Bcd^{085} construct was digested from pBlueScript with BamHI and EcoRI and ligated into pBabr.

The wild-type cad-GAL4 reporter (VT010589, coordinates chr2L: 20767347–20768825) was ordered from the Vienna Drosophila Resource Center (VDRC ID 205848/construct ID 210589). The mutated *cad* enhancer sequence was synthesized by GenScript, amplified, and cloned into the pBPGUw vector (Pfeiffer et al., 2008).

Primers, sequences, and plasmids are available upon request.

Western Blots

Live embryos were dechorionated in bleach, rinsed in salt solution (NaCl with TritonX-100), and embryos at NC14 were sorted under a light microscope and flash frozen on dry ice. Western blots were performed using a using a rabbit anti-GFP antibody

(Millipore Cat # AB3080P) and mouse anti-tubulin antibody (Sigma Cat # T9026) as a loading control. For quantification, the GFP band intensities were normalized to α-tubulin band intensities in each lane. Two biological replicates of 50 embryos were homogenized in 50μL buffer for each genotype, and 10μL (= 10 embryos) was loaded per lane.

Western blots were used to generate an estimate of Bcd concentration in each of the uniform Bcd lines. Drocco, *et al.* used western blots to measure Bcd protein accumulation in the embryo during development, and calculated the total amount of Bcd in the embryo at NC14 to be $1.5\pm0.2\text{x}10^8$ molecules (Drocco et al., 2011). Given that the volume of the nucleus is ~1/10 (or 1/1+9) the volume of the cytoplasm and Bcd partitions between the nucleus and the cytoplasm at a ratio of ~4:1 (Gregor et al., 2007a), we can generate a ratio of 4/4+9 or 0.31 for nuclear/cytoplasmic Bcd. Using this value, we can convert $1.5\pm0.2\text{x}10^8$ molecules/embryo into $4.6\text{x}10^7$ molecules/nucleus at NC14. At this stage, there are 6,000 nuclei at the cortex of the embryo, which would be ~7,750 Bcd molecules/nucleus if the Bcd were distributed uniformly. Additionally, optical measurements estimate a nuclear concentration of Bcd as 8±1 nM and 690 Bcd molecules at the *hunchback* expression boundary (~48% x/L) at NC14 (Gregor et al., 2007b). We used these values to generate a conversion factor of 0.011594203 nM/molecule and calculate the approximate nuclear concentrations given below for each uniform Bcd line. See also Figure 1 Figure Supplement 1D.

Genotype	**Expression/WT**	**Number of Molecules**	**Nuclear Concentration**
bcd>uBcd	0.14	1085	12.58 nM

mtrm>uBcd	1.1	8525	98.84 nM
αTub67C>uBcd	2.7	20925	242.61 nM

Table S1. Estimated nuclear concentrations of Bcd protein in each uniform line.

Immunostaining and Imaging

Embryos of indicated genotypes were collected from 0-4 hour laying cages, and fixed and stained essentially as described in (Dubuis et al., 2013), with rabbit anti-Bcd, guinea pig anti-Kni, and rat anti-Btd primary antibodies, followed by fluorophore-conjugated secondary antibodies Alexa-488 (guinea pig), Alexa-568 (rat), and Alexa-647 (rabbit) from Invitrogen. Stained embryos were imaged on a Leica SP5 laser-scanning confocal microscope.

Live Imaging and Image Analysis

Dechorionated embryos of the indicated genotypes were mounted on coverslips overlaid with halocarbon oil and imaged in the mid-sagittal plane on a Leica SP5 laser scanning confocal microscope. Image analysis was performed in MATLAB (http://www.mathworks.com). GFP intensity along the dorsal profile of each embryo was extracted for each frame of the live movies in nuclear cycle 14. The frame with the highest overall intensity in each movie was plotted.

Bicoid homeodomain expression and protein purification

A cDNA coding for amino acids 89-154 of the Bicoid protein (including the homeodomain) as described in (Burz et al., 1998) with a C-terminal HA epitope tag was cloned into the pET-15b plasmid, which contains an N-terminal 6xHis tag and T7

promoter, to make plasmid pET-15B-BcdHD. Expression was induced in BL21 (DE3) pLysS *E. coli* cells using 2 mM IPTG. The protein was purified by affinity chromatography using HisPur Cobalt Resin (Fisher Scientific Cat # 89965) followed by ion exchange chromatography with SP Sepharose Fast Flow resin (GE Healthcare Cat #17-0729-01).

EMSAs and K_d Calculations

EMSAs were performed using purified Bicoid homeodomain and biotin-labeled DNA probes were designed to span ~200 bp in the maximal peak region of Bcd-bound peaks identified by ChIP and corresponding to previously characterized enhancers. Effective K_d values for each enhancer probe were calculated using the ratio of total shifted probe to free probe.

Primers		**Sequence (5'->3')**
hbP2 probe F	**Forward primer**	/bio/GTCAAGGGATTAGATGGGCA
hbP2 Probe R	**Reverse primer**	/bio/GTCGACTCCTGACCAACGTA
kni post F	**Forward primer**	/bio/AGAAAAAATGAGAACAATGTGAC
kni post R	**Reverse primer**	/bio/AGCCAGCGATTTCGTTACCT
kni ant F	**Forward primer**	/bio/ACAACACCGACCCGTAATCC
kni ant R	**Reverse primer**	/bio/GTCATGTTGGCTAATCTGGC
kr ant F	**Forward primer**	/bio/CAGAAAAGAAAAAGTGTAACGCC

Kr ant R	**Reverse primer**	/bio/GCGAAAAAACGCGTCGCGCT
otd intron F	**Forward primer**	/bio/ATCGTTCCTTGCGGTTTAAT
otd intron R	**Reverse primer**	/bio/AGAACAGGACAAAGGGAATTTAATC
otd early F	**Forward primer**	/bio/CTCGCCTCGCGTGCGACATT
otd early R	**Reverse primer**	/bio/CCTGCGGCAGGACTTCACTT
btd F	**Forward primer**	/bio/ACGAAGTCAAAACTTTTCCA
btd R	**Reverse primer**	/bio/AGCTAAGAGATCTCAACCAAC
gt -3 F	**Forward primer**	/bio/TTACAACTGCCCATTCAGGG
gt -3 R	**Reverse primer**	/bio/GAAGGGCTCGGGTTCGG
gt -10 F	**Forward primer**	/bio/AGATCCAGGCGAGCACTTGA
gt -10 R	**Reverse primer**	/bio/TTAAATTAAAATGTCGCAGGAAGGCG

Table S2: Primer sequences for EMSA probes.

ChIP-seq and Data Analysis

Sample Collection

Drosophila embryos were collected from 0-4 hour laying cages, dechorionated in bleach and crosslinked in with 180 mL 20% paraformaldehyde in 2 ml PBS + 0.5% Triton X-100 and 6 mL Heptane for 15 minutes. Crosslinking was quenched with 125 mM Glycine in PBS + 0.5% Triton X-100. Fixed embryos were visually staged and sorted using a dissecting microscope, and all experimental replicates consisted of 200 embryos in

nuclear cycle 14. Chromatin immunoprecipitation was performed with an anti-GFP antibody (Millipore) in embryos expressing GFP-tagged Bcd either in a wild-type graded distribution (*eGFP-Bcd;;bcd^{E1}* and *eGFP-Bcd;;bcd^{E1} nos^{L7} tsl^{4}*) or uniformly (*GFP-uBcd;;bcd^{E1}*). Sequencing libraries were prepared using the NEBNext ChIP-seq Library Prep master mix kit and sequenced as described in (Blythe and Wieschaus, 2015; Drocco et al., 2011).

Defining a Peak List

Barcode split sequencing files were mapped to *Drosophila melanogaster* genome assembly BDGP R5/dm3 using Bowtie2 (Gregor et al., 2007a; Langmead and Salzberg, 2012) using default parameters. To generate a conservative, high-confidence list of Bcd-bound peaks, peaks were called on each replicate of wild-type and uniform Bcd ChIP-seq data using MACS2 (Gregor et al., 2007b; Zhang et al., 2008) with settings -p 1e-3 --to-large --nomodel --shiftsize 130 for wild-type samples and -p 0.000001 --slocal 5000 --llocal 50000 --keep-dup all for uBcd samples. The most reproducible peaks from each genotype were selected using an irreproducible discovery rate (IDR) of 1% (Dubuis et al., 2013; Landt et al., 2012; Li et al., 2011). Given evidence that highly transcribed (i.e., highly accessible) regions often give false positive results in ChIP experiments (Burz et al., 1998; Teytelman et al., 2013), we used our ATAC-seq data to filter our ChIP-seq peaks. We compared the number of CPM-normalized ATAC-seq reads to ChIP-seq reads in each peak, and performed permutation tests (n = 1,000) to determine the probability of selecting open regions of the genome at random that had higher ATAC-seq counts (i.e., regions that were more accessible) than the ATAC-seq counts in the Bcd ChIP-peaks. We determined that at a ratio of 5.4 ATAC-seq/ChIP-seq

counts, 95% of the ChIP peaks (permutation test p value = 0.05) were no more open than a random selection of open regions. We filtered out the remaining ChIP peaks with ATAC/ChIP ratios above 5.4, as these peaks are more likely to correspond to highly transcribed open regions where most false positive signals can be found. We then chose the peaks that were common to wild-type and uniform Bcd embryos, which resulted in a list of 1,027 Bcd-bound peak regions. The number of peaks at each step of this filtering is shown in Table S3.

	Number of Peaks			
Filter Applied	**Wild-Type**	**tub>uBcd**	**mtrm>uBcd**	**bcd>uBcd**
MACS2	29,090	15,429	11,812	38,392
IDR	9,815	4,245	1,464	1,329
Euchromatic only	2,319	4,123	1,429	1,257
Common peaks (2/3)		4,126		
ATAC-seq ratios	2,143	2,087		
Common Peaks	1,027			

Table S3. Number Bcd ChIP-seq peaks at each step of filtering.

Comparing Binding Between Uniform Bcd Levels

Mapped BAM files were imported into R as GenomicRanges objects (Lawrence et al., 2013), filtering out reads with map quality scores below 30. Significant differences between the uBcd levels were assessed on a pairwise basis using edgeR (Robinson et al., 2010) in the 1,027 pre-defined peak plus 50,000 additional non-peak noise regions selected from the dm3 genome.

Data Normalization and Display

Sequencing data was z-score normalized for display in heatmaps. Sequencing read count coverage was calculated for 10 base pair windows across the genome, and the mean counts per million reads were determined in each ChIP peak, as well as the additional noise peaks. Z-scores were computed for each peak using

$$z = \frac{CPM - \mu}{\sigma}$$

where μ = mean CPM in noise peaks and σ = standard deviation of CPM in noise peaks.

Overlaps with Vienna Tile-GAL4 Enhancers

	Overlaps		Total Vienna Tiles
	Bcd Peaks	**Vienna Tiles**	
Expressed (all stages)	193	238	3604
Expressed (stage 4-6)	151	163	666
Not Expressed	41	55	4189
Total	234	293	7793

Table S4. Number of overlapping Bcd ChIP peaks and Vienna Tile-GAL4 enhancer reporters. The reporters expressed at stage 4-6 that overlapped with more than one Bcd peak were excluded from the plot in Figure 2B.

ATAC-seq and Data Analysis

Sample Collection

Live embryos expressing a histone (H2Av)-GFP or RFP construct were individually staged on an epifluorescence microscope in halocarbon oil. After the onset of nuclear cycle 14, single embryos were dechorionated in bleach and macerated in cold lysis buffer at t = 12 minutes into NC14. Samples were pelleted in lysis buffer at 4°C (3000 rpm for 10 minutes), buffer was removed, and the embryo pellet was flash frozen on dry

ice. Frozen pellets were resuspended in Nextera Tagment DNA Buffer + Enzyme and incubated at 37°C for 30 minutes shaking at 800 rpm. Tagged DNA was purified using a Qiagen Minelute column and eluted in 10 µL. Barcoded sequencing libraries were generated by PCR amplifying the purified DNA using the Nextera DNA Sample Prep kit. Paired-end sequencing was performed on six samples per genotype by the Lewis Sigler Institute for Integrative Genomics Sequencing Core Facility on an Illumina HiSeq 2500.

Data Processing

Initial processing of the data was performed essentially as described in (Blythe and Wieschaus 2016, *submitted*). Sequencing files were barcode split and adaptors were trimmed using TrimGalore. Trimmed reads were mapped to the BDGP R5/dm3 genome assembly using BWA (Li and Durbin, 2009) with default parameters. Optical and PCR duplicates were marked using Picard Tools MarkDuplicates (https://broadinstitute.github.io/picard/). Mapped reads were filtered using samtools (Li et al., 2009) to remove reads with a map quality score ≤ 30, unmapped reads, improperly paired reads, and duplicate reads. To distinguish reads corresponding to open chromatin reads from nucleosome protected reads, the size of the ATAC-seq fragments were fit to the sum of an exponential and Gaussian distribution as described in (Buenrostro et al., 2013). We used a fragment size cutoff of ≤ 100 bp to identify fragments originating from open chromatin. Filtered open reads were imported into R as GenomicRanges objects.

Peak Calling

Regions of open chromatin at NC14+12 minutes were determined by calling peaks on the merged open chromatin reads from wild-type replicates using Zinba (Rashid et al., 2011) with the parameters:

input = 'none', winSize = 300, offset = 50, extension = 65, selectmodel = FALSE, formula = exp_count ~ exp_cnvwin_log + align_perc, formulaE = exp_count ~ exp_cnvwin_log + align_perc, formulaZ = exp_count ~ align_perc, FDR = TRUE, threshold = 0.05, winGap = 0, cnvWinSize = 2.5E+4, refinepeaks = TRUE.

Nucleosome Positioning

Nucleosome positioning was determined samples from all genotypes using NucleoATAC (Schep et al., 2015), with default settings. Peak regions used for NucleoATAC were open chromatin peaks from Zinba combined with the Bcd ChIP peaks and widened to 2500 bp centered over the peak maxima. This combined peak list was then reduced and used as NucleoATAC input. For each genotype, BAM files from ATAC-seq were merged and used as input for NucleoATAC.

Differential Accessibility between Wild-Type, bcd^{E1}, zld^{-} Embryos

EdgeR was used to determine significant differences in accessibility between different genotypes, with an exact test FDR ≤ 0.05 used as the significance cutoff. For edgeR comparisons, the ATAC-seq peaks called by Zinba from wild-type embryos at NC14+12 minutes were combined with Bcd ChIP-seq peaks resized to 300 bp centered around the peak summit and 25,000 background regions. The background regions were generated by extending each of the ATAC open peaks to 10 kb and subtracting them from the dm3 genome assembly. The remaining non-peak regions were then sampled randomly 25,000 times and widened to reflect the distribution of sizes in the ATAC-seq

peaks. Bcd- or Zld-dependent peaks were those peaks identified as having reduced accessibility *bcd*^{E1} or *zld*$^{-}$ embyos. A summary of the differential accessibility in the ATAC-seq vs. Bcd ChIP-seq peaks is shown in Table S5.

Peak List	Bcd Dependent	Zld Dependent	Bcd+Zld Dependent	Total
ATAC Open Peaks	326	2,675	206	13,226
Bcd ChIP Peaks	132	402	61	1,027
ATAC+ChIP Common Peaks	121	379	58	855

Table S5. Number of peaks dependent on Bcd or Zld for chromatin accessibility. ATAC + ChIP common peaks are peaks that overlap between the Bcd ChIP-seq peaks and the wild-type ATAC-seq open chromatin peaks.

To measure differential accessibility of Bcd motifs between wild type and bcdE1 mutant embryos, the positions of Bcd motifs within ChIP-seq peaks were found, and ATAC-seq accessibility scores were calculated for the 10 bp window containing the midpoint of each Bcd motif. Scores for all motifs within a single peak were averaged prior to plotting. Motifs were found using the “strong” Bcd position weight matrix via the R function ‘matchPWM’ in the Biostrings package with an 80% match threshold.

To estimate the overlap between nucleosomes and Bcd motifs, predicted nucleosome dyad centers from NucleoATAC were widened to 160 bp and motifs overlapping these intervals were scored as ‘nucleosome associated’. Motifs not overlapping widened nucleosome intervals were scored as ‘open’. The fraction of open Bcd motifs per peak was calculated by dividing the number of open Bcd motifs by the total number of encoded Bcd motifs over each peak.

776

777 ***Data Normalization and Display***

778 For each genotype, BAM-formatted ATAC-seq reads for each replicate, filtered by
779 quality and duplicates removed as described above, were merged into a single file.
780 Coverage was calculated from these BAM files in 10 bp windows in the dm3 genome
781 assembly. This coverage was then normalized by counts per million reads. The genome
782 coverage in 2 kb regions flanking Bcd ChIP peaks was then z-score normalized as
783 described above. The z-score values are displayed as heatmaps of open chromatin
784 displayed in Figure 3 A and B. Heatmaps are plotted in order of decreasing accessibility
785 z score in wild-type embryos.
786 Predicted dyad centers from NucleoATAC were widened to 147 bp to model
787 nucleosome positions. Occupancy scores from NulcleoATAC in the 147 bp
788 nucleosomes were computed in 10 bp windows across the dm3 genome assembly.
789 Occupancy scores overlapping Bcd ChIP peaks are plotted in the heatmaps in Fig 4 A
790 and B. Nucleosome heatmaps are plotted in the same order as open chromatin
791 heatmaps, by decreasing accessibility z score in wild-type embryos.

792

793 Supplemental File 1 shows the genomic (BDGP Release 5/dm3) coordinates of Bcd-
794 bound peaks identified by ChIP-seq as described in Table S3. Additional columns
795 indicate the nearest gene to the peak that shows maternal or zygotic expression in the
796 embryo (Blythe and Wieschaus, 2015) and classifications of each peak as Bcd or Zld
797 dependent for accessibility (determined by ATAC-seq) and their sensitivity group
798 classifications (determined by ChIP-seq). The tileID column gives the name of each

Vienna Tile-GAL4 construct (if any) that overlaps with each peak, and the HC_ID column indicates reporter constructs from (Chen, et al., 2012) that overlap with each peak.

In situ hybridizations and Cad-GAL4 reporters

The GAL4 coding sequence was amplified from a genomic DNA preparation generated from a *Drosophila* stock carrying a GAL4 reporter, using primers 5'-TGCGATATTTGCCGACTTA-3' and 5'-TGTAATACGACTCACTATAGGGAACATCCCTGTAGTGATTCCA-3'. The amplified sequence was used as a template in the MEGAscript T7 Transcription Kit (ThermoFisher Cat. #AM1334) to with digoxygenin-labeled UTP to generate an anti-GAL4 RNA probe. *In situ* hybridizations were performed according to standard protocols.

Author Contributions

C.E.H and S.A.B. designed experiments. C.E.H. performed all experiments and C.E.H. and S.A.B. performed data analysis. E.F.W. discussed results and performed difficult meiotic recombination. C.E.H. wrote the first draft of the manuscript and S.A.B. and E.F.W. contributed to the final version.

Acknowledgements

We thank T. Gregor, E. Gavis, O. Grimm, and members of the Wieschaus and Schüpbach labs for helpful feedback and discussion, H. Chen, M. Levine and S. Little

822 for comments on the manuscript, and W. Wang and the staff of the Lewis-Sigler Institute
823 Sequencing Core Facility. This work was supported by Ruth L. Kirschstein NRSA pre-
824 doctoral fellowship F31HD082940 (C.E.H.) and postdoctoral fellowship F32HD072653
825 (S.A.B.).

826

References

Amin, S., Neijts, R., Simmini, S., van Rooijen, C., Tan, S.C., Kester, L., van Oudenaarden, A., Creyghton, M.P., and Deschamps, J. (2016). Cdx and T Brachyury Co-activate Growth Signaling in the Embryonic Axial Progenitor Niche. Cell Rep *17*, 3165–3177.

Berleth, T., Burri, M., Thoma, G., Bopp, D., Richstein, S., Frigerio, G., Noll, M., and Nüsslein-Volhard, C. (1988). The role of localization of bicoid RNA in organizing the anterior pattern of the Drosophila embryo. Embo J. *7*, 1749–1756.

Blythe, S.A., and Wieschaus, E.F. (2015). Zygotic Genome Activation Triggers the DNA Replication Checkpoint at the Midblastula Transition. Cell *160*, 1–13.

Bosch, ten, J.R., Benavides, J.A., and Cline, T.W. (2006). The TAGteam DNA motif controls the timing of Drosophila pre-blastoderm transcription. Development *133*, 1967–1977.

Buenrostro, J.D., Giresi, P.G., Zaba, L.C., Chang, H.Y., and Greenleaf, W.J. (2013). Transposition of native chromatin for fast and sensitive epigenomic profiling of open chromatin, DNA-binding proteins and nucleosome position. Nat. Methods *10*, 1213–1218.

Buenrostro, J.D., Wu, B., Chang, H.Y., and Greenleaf, W.J. (2015). ATAC-seq: A Method for Assaying Chromatin Accessibility Genome-Wide. Curr Protoc Mol Biol *109*, 21.29.1–.29.9.

Burz, D.S., and Hanes, S.D. (2001). Isolation of mutations that disrupt cooperative DNA binding by the Drosophila bicoid protein. J. Mol. Biol. *305*, 219–230.

Burz, D.S., Rivera-Pomar, R., Jäckle, H., and Hanes, S.D. (1998). Cooperative DNA-binding by Bicoid provides a mechanism for threshold-dependent gene activation in the Drosophila embryo. Embo J. *17*, 5998–6009.

Chan, H.M., and La Thangue, N.B. (2001). p300/CBP proteins: HATs for transcriptional bridges and scaffolds. J. Cell. Sci. *114*, 2363–2373.

Chen, H., Xu, Z., Mei, C., Yu, D., and Small, S. (2012). A System of Repressor Gradients Spatially Organizes the Boundaries of Bicoid-Dependent Target Genes. Cell *149*, 618–629.

Crauk, O., and Dostatni, N. (2005). Bicoid Determines Sharp and Precise Target Gene Expression in the Drosophila Embryo. Current Biology *15*, 1888–1898.

De Renzis, S., Elemento, O., Tavazoie, S., and Wieschaus, E.F. (2007). Unmasking Activation of the Zygotic Genome Using Chromosomal Deletions in the Drosophila Embryo. PLoS Biol. *5*, e117.

862 Driever, W., and Nüsslein-Volhard, C. (1988a). The bicoid protein determines position in
863 the Drosophila embryo in a concentration-dependent manner. Cell *54*, 95–104.

864 Driever, W., and Nüsslein-Volhard, C. (1989). The bicoid protein is a positive regulator
865 of hunchback transcription in the early Drosophila embryo. Nature *337*, 138–143.

866 Driever, W., Ma, J., Nüsslein-Volhard, C., and Ptashne, M. (1989a). Rescue of bicoid
867 mutant Drosophila embryos by bicoid fusion proteins containing heterologous activating
868 sequences. Nature *342*, 149–154.

869 Driever, W., and Nüsslein-Volhard, C. (1988b). A gradient of bicoid protein in Drosophila
870 embryos. Cell *54*, 83–93.

871 Driever, W., Thoma, G., and Nüsslein-Volhard, C. (1989b). Determination of spatial
872 domains of zygotic gene expression in the Drosophila embryo by the affinity of binding
873 sites for the bicoid morphogen. Nature *340*, 363–367.

874 Drocco, J.A., Grimm, O., Tank, D.W., and Wieschaus, E. (2011). Measurement and
875 Perturbation of Morphogen Lifetime: Effects on Gradient Shape. Biophysical Journal
876 *101*, 1807–1815.

877 Dubuis, J.O., Samanta, R., and Gregor, T. (2013). Accurate measurements of dynamics
878 and reproducibility in small genetic networks. Molecular Systems Biology *9*, 1–15.

879 Frohnhöfer, H.G., and Nüsslein-Volhard, C. (1986). Organization of anterior pattern in
880 the Drosophila embryo by the maternal gene bicoid. Nature *324*, 120–125.

881 Fu, D., and Ma, J. (2005). Interplay between positive and negative activities that
882 influence the role of Bicoid in transcription. Nucleic Acids Res. *33*, 3985–3993.

883 Fu, D., Wen, Y., and Ma, J. (2004). The co-activator CREB-binding protein participates
884 in enhancer-dependent activities of bicoid. J. Biol. Chem. *279*, 48725–48733.

885 Gao, Q., and Finkelstein, R. (1998). Targeting gene expression to the head: the
886 Drosophila orthodenticle gene is a direct target of the Bicoid morphogen. Development
887 *125*, 4185–4193.

888 Goto, T., Macdonald, P., and Maniatis, T. (1989). Early and late periodic patterns of
889 even skipped expression are controlled by distinct regulatory elements that respond to
890 different spatial cues. Cell *57*, 413–422.

891 Gregor, T., Wieschaus, E.F., McGregor, A.P., and Bialek, W. (2007a). Stability and
892 Nuclear Dynamics of the Bicoid Morphogen Gradient. Cell *130*, 141–152.

893 Gregor, T., Tank, D.W., Wieschaus, E.F., and Bialek, W. (2007b). Probing the limits to
894 positional information. Cell *130*, 153–164.

895 Harrison, M.M., Li, X.-Y., Kaplan, T., Botchan, M.R., and Eisen, M.B. (2011). Zelda

binding in the early Drosophila melanogaster embryo marks regions subsequently activated at the maternal-to-zygotic transition. PLoS Genet. *7*, e1002266.

Häder, T., Wainwright, D., Shandala, T., Saint, R., Taubert, H., Brönner, G., and Jäckle, H. (2000). Receptor tyrosine kinase signaling regulates different modes of Groucho-dependent control of Dorsal. Curr. Biol. *10*, 51–54.

Hoch, M., Seifert, E., and Jäckle, H. (1991). Gene expression mediated by cis-acting sequences of the Krüppel gene in response to the Drosophila morphogens bicoid and hunchback. Embo J. *10*, 2267–2278.

Jaeger, J. (2010). The gap gene network. Cell. Mol. Life Sci. *68*, 243–274.

Janody, F., Sturny, R., Catala, F., Desplan, C., and Dostatni, N. (2000). Phosphorylation of bicoid on MAP-kinase sites: contribution to its interaction with the torso pathway. Development *127*, 279–289.

Janody, F., Sturny, R., Schaeffer, V., Azou, Y., and Dostatni, N. (2001). Two distinct domains of Bicoid mediate its transcriptional downregulation by the Torso pathway. Development *128*, 2281–2290.

Kvon, E.Z., Kazmar, T., Stampfel, G., Yáñez-Cuna, J.O., Pagani, M., Schernhuber, K., Dickson, B.J., and Stark, A. (2014). Genome-scale functional characterization of Drosophila developmental enhancers in vivo. Nature.

Landt, S.G., Marinov, G.K., Kundaje, A., Kheradpour, P., Pauli, F., Batzoglou, S., Bernstein, B.E., Bickel, P., Brown, J.B., Cayting, P., et al. (2012). ChIP-seq guidelines and practices of the ENCODE and modENCODE consortia. Genome Res. *22*, 1813–1831.

Langmead, B., and Salzberg, S.L. (2012). Fast gapped-read alignment with Bowtie 2. Nat. Methods *9*, 357–359.

Lawrence, M., Huber, W., Pagès, H., Aboyoun, P., Carlson, M., Gentleman, R., Morgan, M.T., and Carey, V.J. (2013). Software for computing and annotating genomic ranges. PLoS Comput. Biol. *9*, e1003118.

Levine, M., and Davidson, E.H. (2005). Gene regulatory networks for development. Proceedings of the National Academy of Sciences *102*, 4936–4942.

Li, H., Handsaker, B., Wysoker, A., Fennell, T., Ruan, J., Homer, N., Marth, G., Abecasis, G., Durbin, R., 1000 Genome Project Data Processing Subgroup (2009). The Sequence Alignment/Map format and SAMtools. Bioinformatics *25*, 2078–2079.

Li, H., and Durbin, R. (2009). Fast and accurate short read alignment with Burrows-Wheeler transform. Bioinformatics *25*, 1754–1760.

Li, Q., Brown, J.B., Huang, H., and Bickel, P.J. (2011). Measuring Reproducibility of

931 High-Throughput Experiments. The Annals of Applied Statistics *5*, 1752–1779.

932 Li, X.-Y., MacArthur, S., Bourgon, R., Nix, D., Pollard, D.A., Iyer, V.N., Hechmer, A.,
933 Simirenko, L., Stapleton, M., Luengo Hendriks, C.L., et al. (2008). Transcription factors
934 bind thousands of active and inactive regions in the Drosophila blastoderm. PLoS Biol.
935 *6*, e27.

936 Liu, F., Morrison, A.H., and Gregor, T. (2013). Dynamic interpretation of maternal inputs
937 by the Drosophila segmentation gene network. Proc Natl Acad Sci U S A *110*, 6724–
938 6729.

939 Löhr, U., Chung, H.-R., Beller, M., and Jäckle, H. (2009). Antagonistic action of Bicoid
940 and the repressor Capicua determines the spatial limits of Drosophila head gene
941 expression domains. Proceedings of the National Academy of Sciences *106*, 21695–
942 21700.

943 Ma, X. (1996). Sequences Outside the Homeodomain of Bicoid Are Required for
944 Protein-Protein Interaction. Journal of Biological Chemistry *271*, 21660–21665.

945 Ma, X., Yuan, D., Diepold, K., Scarborough, T., and Ma, J. (1996). The Drosophila
946 morphogenetic protein Bicoid binds DNA cooperatively. Development *122*, 1195–1206.

947 MacArthur, S., Li, X.-Y., Li, J., Brown, J.B., Chu, H.C., Zeng, L., Grondona, B.P.,
948 Hechmer, A., Simirenko, L., Keränen, S.V., et al. (2009). Developmental roles of 21
949 Drosophila transcription factors are determined by quantitative differences in binding to
950 an overlapping set of thousands of genomic regions. Genome Biol. *10*, R80.

951 Mirny, L.A. (2010). Nucleosome-mediated cooperativity between transcription factors.
952 Proceedings of the National Academy of Sciences *107*, 22534–22539.

953 Nien, C.-Y., Liang, H.-L., Butcher, S., Sun, Y., Fu, S., Gocha, T., Kirov, N., Manak, J.R.,
954 and Rushlow, C. (2011). Temporal coordination of gene networks by Zelda in the early
955 Drosophila embryo. PLoS Genet. *7*, e1002339.

956 Ochoa-Espinosa, A., Yu, D., Tsirigos, A., Struffi, P., and Small, S. (2009). Anterior-
957 posterior positional information in the absence of a strong Bicoid gradient. Proceedings
958 of the National Academy of Sciences *106*, 3823–3828.

959 Ochoa-Espinosa, A., Yucel, G., Kaplan, L., Pare, A., Pura, N., Oberstein, A.,
960 Papatsenko, D., and Small, S. (2005). The role of binding site cluster strength in Bicoid-
961 dependent patterning in Drosophila. Proc Natl Acad Sci U S A *102*, 4960–4965.

962 Pankratz, M.J., Busch, M., Hoch, M., Seifert, E., and Jäckle, H. (1992). Spatial control of
963 the gap gene knirps in the Drosophila embryo by posterior morphogen system. Science
964 *255*, 986–989.

965 Perry, M.W., Boettiger, A.N., and Levine, M. (2011). Multiple enhancers ensure
966 precision of gap gene-expression patterns in the Drosophila embryo. Proc Natl Acad Sci

967 U S A *108*, 13570–13575.

968 Pfeiffer, B.D., Jenett, A., Hammonds, A.S., Ngo, T.-T.B., Misra, S., Murphy, C., Scully,
969 A., Carlson, J.W., Wan, K.H., Laverty, T.R., et al. (2008). Tools for neuroanatomy and
970 neurogenetics in Drosophila. Proceedings of the National Academy of Sciences *105*,
971 9715–9720.

972 Rashid, N.U., Giresi, P.G., Ibrahim, J.G., Sun, W., and Lieb, J.D. (2011). ZINBA
973 integrates local covariates with DNA-seq data to identify broad and narrow regions of
974 enrichment, even within amplified genomic regions. Genome Biol. *12*, R67.

975 Rechsteiner, M., and Rogers, S.W. (1996). PEST sequences and regulation by
976 proteolysis. Trends Biochem. Sci. *21*, 267–271.

977 Rivera-Pomar, R., Niessing, D., Schmidt-Ott, U., Gehring, W.J., and Jäckle, H. (1996).
978 RNA binding and translational suppression by bicoid. Nature *379*, 746–749.

979 Robinson, M.D., McCarthy, D.J., and Smyth, G.K. (2010). edgeR: a Bioconductor
980 package for differential expression analysis of digital gene expression data.
981 Bioinformatics *26*, 139–140.

982 Sauer, F., Hansen, S.K., and Tjian, R. (1995). DNA Template and Activator-Coactivator
983 Requirements for Transcriptional Synergism by Drosophila Bicoid. Science *270*, 1825–
984 1828.

985 Schep, A.N., Buenrostro, J.D., Denny, S.K., Schwartz, K., Sherlock, G., and Greenleaf,
986 W.J. (2015). Structured nucleosome fingerprints enable high-resolution mapping of
987 chromatin architecture within regulatory regions. Genome Res. *25*, 1757–1770.

988 Schroeder, M.D., Pearce, M., Fak, J., Fan, H., Unnerstall, U., Emberly, E., Rajewsky,
989 N., Siggia, E.D., and Gaul, U. (2004). Transcriptional control in the segmentation gene
990 network of Drosophila. PLoS Biol. *2*, E271.

991 Segal, E., Fondufe-Mittendorf, Y., Chen, L., Thåström, A., Field, Y., Moore, I.K., Wang,
992 J.-P.Z., and Widom, J. (2006). A genomic code for nucleosome positioning. Nature *442*,
993 772–778.

994 Segal, E., Raveh-Sadka, T., Schroeder, M., Unnerstall, U., and Gaul, U. (2008).
995 Predicting expression patterns from regulatory sequence in Drosophila segmentation.
996 Nature *451*, 535–540.

997 Struhl, G., Struhl, K., and Macdonald, P.M. (1989). The gradient morphogen bicoid is a
998 concentration-dependent transcriptional activator. Cell *57*, 1259–1273.

999 Sun, Y., Nien, C.-Y., Chen, K., Liu, H.-Y., Johnston, J., Zeitlinger, J., and Rushlow, C.
1000 (2015). Zelda overcomes the high intrinsic nucleosome barrier at enhancers during
1001 Drosophila zygotic genome activation. Genome Res. *25*, 1703–1714.

1002 Teytelman, L., Thurtle, D.M., Rine, J., and van Oudenaarden, A. (2013). Highly
1003 expressed loci are vulnerable to misleading ChIP localization of multiple unrelated
1004 proteins. Proceedings of the National Academy of Sciences *110*, 18602–18607.

1005 Thomas-Chollier, M., Herrmann, C., Defrance, M., Sand, O., Thieffry, D., and van
1006 Helden, J. (2012). RSAT peak-motifs: motif analysis in full-size ChIP-seq datasets.
1007 Nucleic Acids Res. *40*, e31.

1008 Thomas-Chollier, M., Sand, O., Turatsinze, J.-V., Janky, R., Defrance, M., Vervisch, E.,
1009 Brohée, S., and van Helden, J. (2008). RSAT: regulatory sequence analysis tools.
1010 Nucleic Acids Res. *36*, W119–W127.

1011 Wang, X., Bai, L., Bryant, G.O., and Ptashne, M. (2011). Nucleosomes and the
1012 accessibility problem. Trends Genet. *27*, 487–492.

1013 Wimmer, E.A., Simpson-Brose, M., Cohen, S.M., Desplan, C., and Jäckle, H. (1995).
1014 Trans- and cis-acting requirements for blastodermal expression of the head gap gene
1015 buttonhead. Mech. Dev. *53*, 235–245.

1016 Wolpert, L. (1969). Positional information and the spatial pattern of cellular
1017 differentiation. Journal of Theoretical Biology *25*, 1–47.

1018 Xi, L., Fondufe-Mittendorf, Y., Xia, L., Flatow, J., Widom, J., and Wang, J.-P. (2010).
1019 Predicting nucleosome positioning using a duration Hidden Markov Model. BMC
1020 Bioinformatics *11*, 346.

1021 Xu, Z., Chen, H., Ling, J., Yu, D., Struffi, P., and Small, S. (2014). Impacts of the
1022 ubiquitous factor Zelda on Bicoid-dependent DNA binding and transcription in
1023 Drosophila. Genes Dev. *28*, 608–621.

1024 Zhang, Y., Liu, T., Meyer, C.A., Eeckhoute, J., Johnson, D.S., Bernstein, B.E.,
1025 Nusbaum, C., Myers, R.M., Brown, M., Li, W., et al. (2008). Model-based analysis of
1026 ChIP-Seq (MACS). Genome Biol. *9*, R137.

1027 Zhao, C., Fu, D., Dave, V., and Ma, J. (2003). A composite motif of the Drosophila
1028 morphogenetic protein bicoid critical to transcription control. J. Biol. Chem. *278*, 43901–
1029 43909.

1030 Zhu, W., Foehr, M., Jaynes, J.B., and Hanes, S.D. (2001). Drosophila SAP18, a
1031 member of the Sin3/Rpd3 histone deacetylase complex, interacts with Bicoid and
1032 inhibits its activity. Development Genes and Evolution *211*, 109–117.

1033

1034

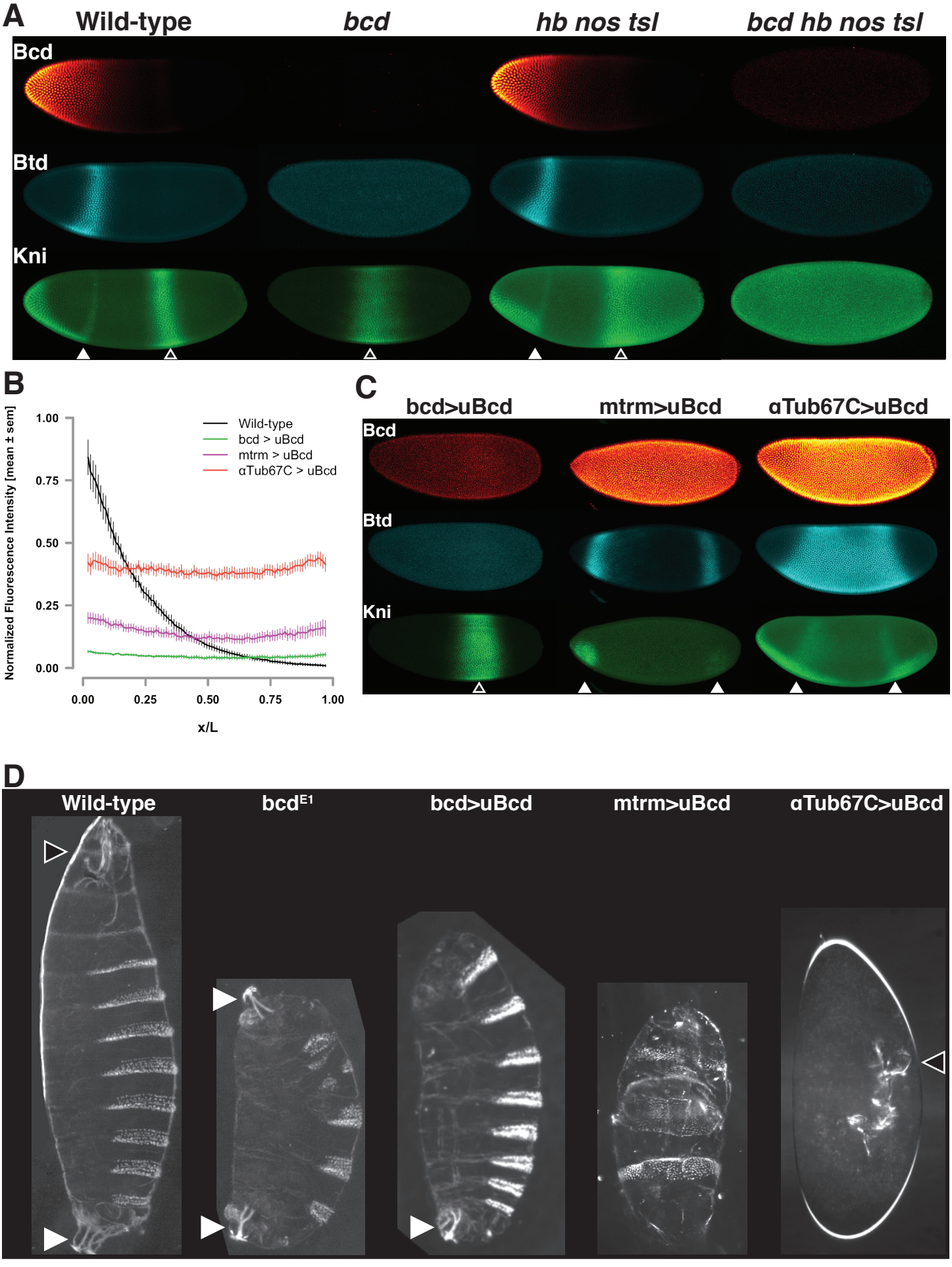

Figure 1. Uniform Bcd expression specifies cell fates corresponding to levels of expression.

(A) Wild-type, *bcd* null mutant (*bcd*^{E1}), and maternal *hunchback, nanos, torso-like (hb nos tsl)* triple mutant and *bcd hb nos tsl* mutant embryos at NC14 immunostained with antibodies against Bcd, Btd, and Kni. Embryos are oriented with anterior to the left. The anterior Kni domain (filled arrow) is absent in *bcd* but restored in *hb nos tsl* embryos, while the posterior stripe (open arrow) shifts anteriorly in in *bcd* but expands posteriorly in *hb nos tsl.* Neither Btd nor Kni exhibit patterned expression in *bcd hb nos tsl*. Images are maximum z-projections and image contrast was adjusted uniformly across the entire image for display. See Figure S1A for quantification of Kni intensity between genotypes.

(B) Expression levels of uniform GFP-Bcd transgenic constructs relative to wild-type Bcd expression. Live embryos were imaged in during NC14, and dorsal profiles were plotted. Error bars are standard error of the mean. For wild-type, n = 23 embryos; bcd-uBcd n = 13; mtrm-uBcd n = 7; and αTub67C -uBcd n = 14. See also Figures S1 and S2 and Table S1.

(C) Immunostaining as (A), for each level of uniform Bcd. Anterior target gene expression is absent at the lowest level. At intermediate (*mtrm*) and high (*αTub67C*) levels of uBcd, anterior expression patterns are expanded and/or duplicated in the posterior, and posterior expression of Kni is absent.

(D) Larval cuticle preparations for the indicated genotypes. Embryos are oriented with anterior at the top. Head structures are indicated with open arrows and tail structures with filled arrows. *αTub67C*>uBcd embryos develop essentially no cuticle tissue, but form only what appear to be anteriorly-derived mouth structures. mtrm>uBcd results in a

duplication of the anterior-most abdominal denticles in the anterior and posterior of the embryo, with no clear terminal structures forming at either end. bcd>uBcd embryos have a normal posterior and all abdominal segments, but no thoracic or head structures. Images of individual embryos were rotated and cropped to exclude nearby embryos and air bubbles.

A

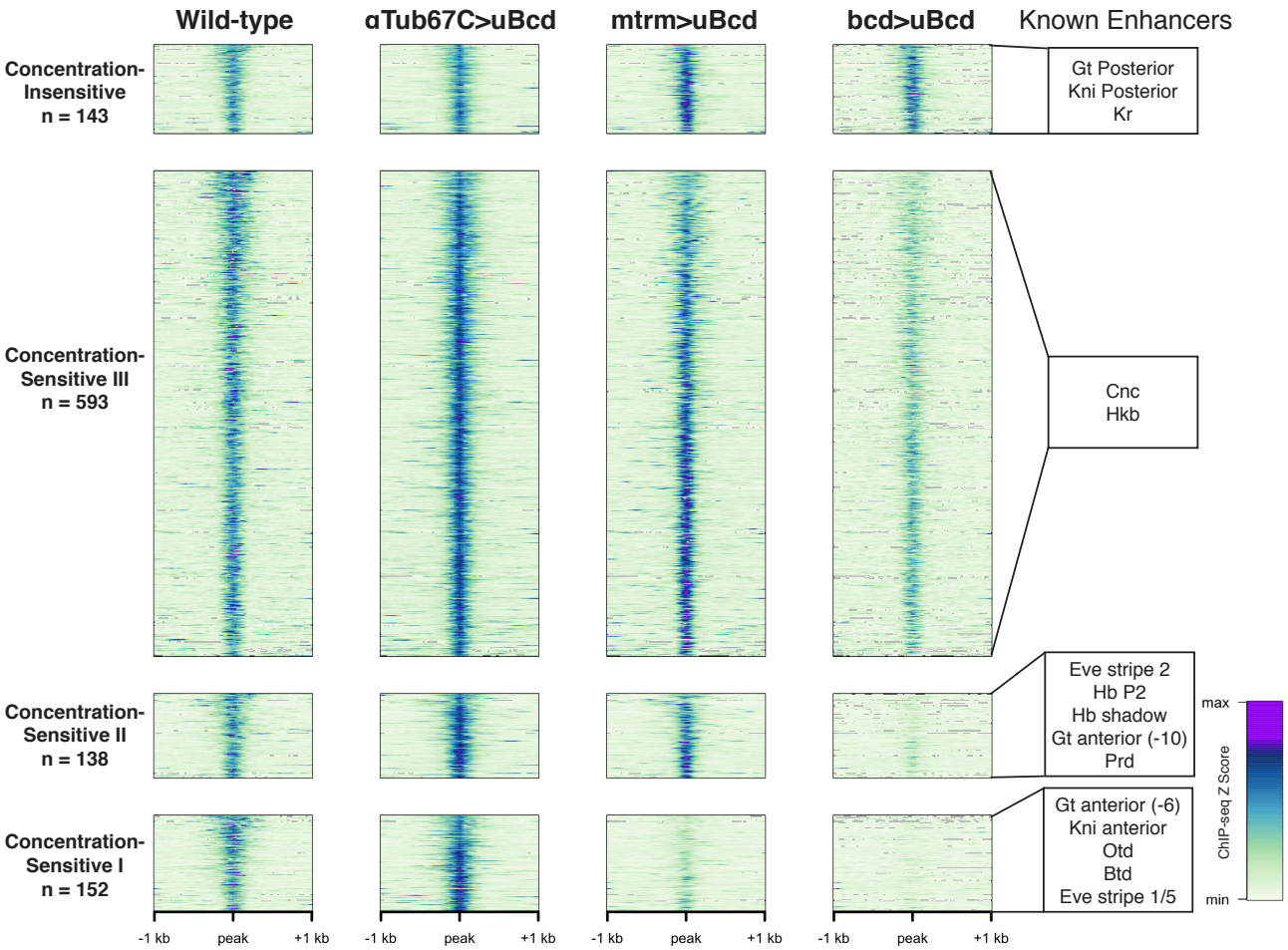

B

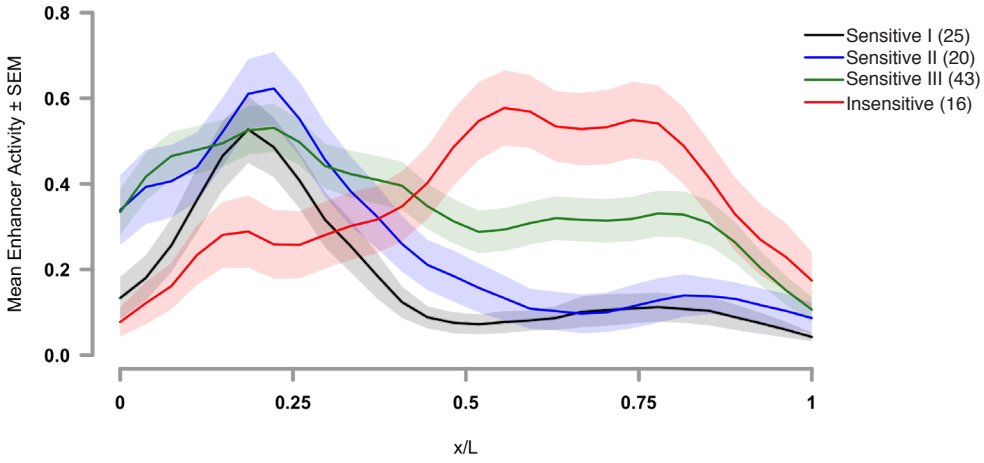

C

Transcription Factor	Discovered Motif	e-value	# of sites
Zld	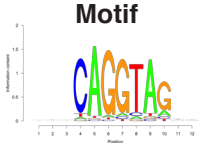	8.5×10^{-91}	1783
Bcd (Strong)	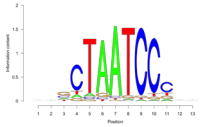	4.6×10^{-67}	1273
Bcd (Weak)	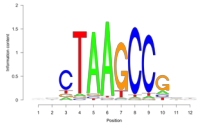	1.6×10^{-53}	880

D

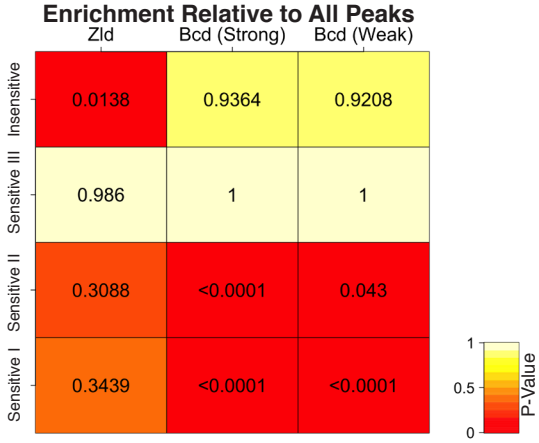

Figure 2. Bcd-bound regions are classified into groups of increasing sensitivity to Bcd concentration.

(A) ChIP-seq data in Bcd-bound peaks. Data is displayed as a heatmap of z-score normalized ChIp-seq reads, in a 2 kb region centered around each peak. Peaks in each class are arranged in order of decreasing z-scores in wild-type embryos. One peak (peak 549, see Table S6) was not classified, as it showed increasing binding at decreasing Bcd concetrations. Previously characterized enhancers overlapping with each class are indicated at right. Concentration-Insensitive: the posterior stripe enhancers for both *knirps* (Pankratz et al., 1992) and *giant* (Schroeder et al., 2004), and the *Kr* CD1 enhancer (Hoch et al., 1991).

Concentration-Sensitive III: *cap'n'collar* (Schroeder et al., 2004), and *huckebein* (Häder et al., 2000) enhancers.

Concentration-Sensitive II: the *hunchback* P2 proximal (Struhl et al., 1989) and shadow enhancers (Perry et al., 2011), the *even-skipped* stripe 2 enhancer (Goto et al., 1989), an early *paired* enhancer (Ochoa-Espinosa et al., 2005), and an anterior enhancer for *giant* (Schroeder et al., 2004).

Concentration-Sensitive I: *buttonhead* (Wimmer et al., 1995)*, orthodenticle* (Gao and Finkelstein, 1998)*,* and anterior enhancers for both *knirps* and *giant* (Schroeder et al., 2004)*.*

(B) Mean expression patterns of Vienna Tile-GAL4 enhancer reporters overlapping with Bcd peaks in each sensitivity class. Peaks and tiles with more than one overlap were excluded from the plot.

(C) Top DNA motifs discovered by RSAT peak-motifs. The e-value for is a p-value computed from a binomial distribution for a given motif in the dataset, corrected for multiple testing. See Figure S2B for *de novo* motif discovery in each sensitivity class. (D) Heatmap displaying the enrichment of a given motif in each sensitivity class, relative to the peak list as a whole. P-values were generated from permutation tests (n = 10,000 tests).

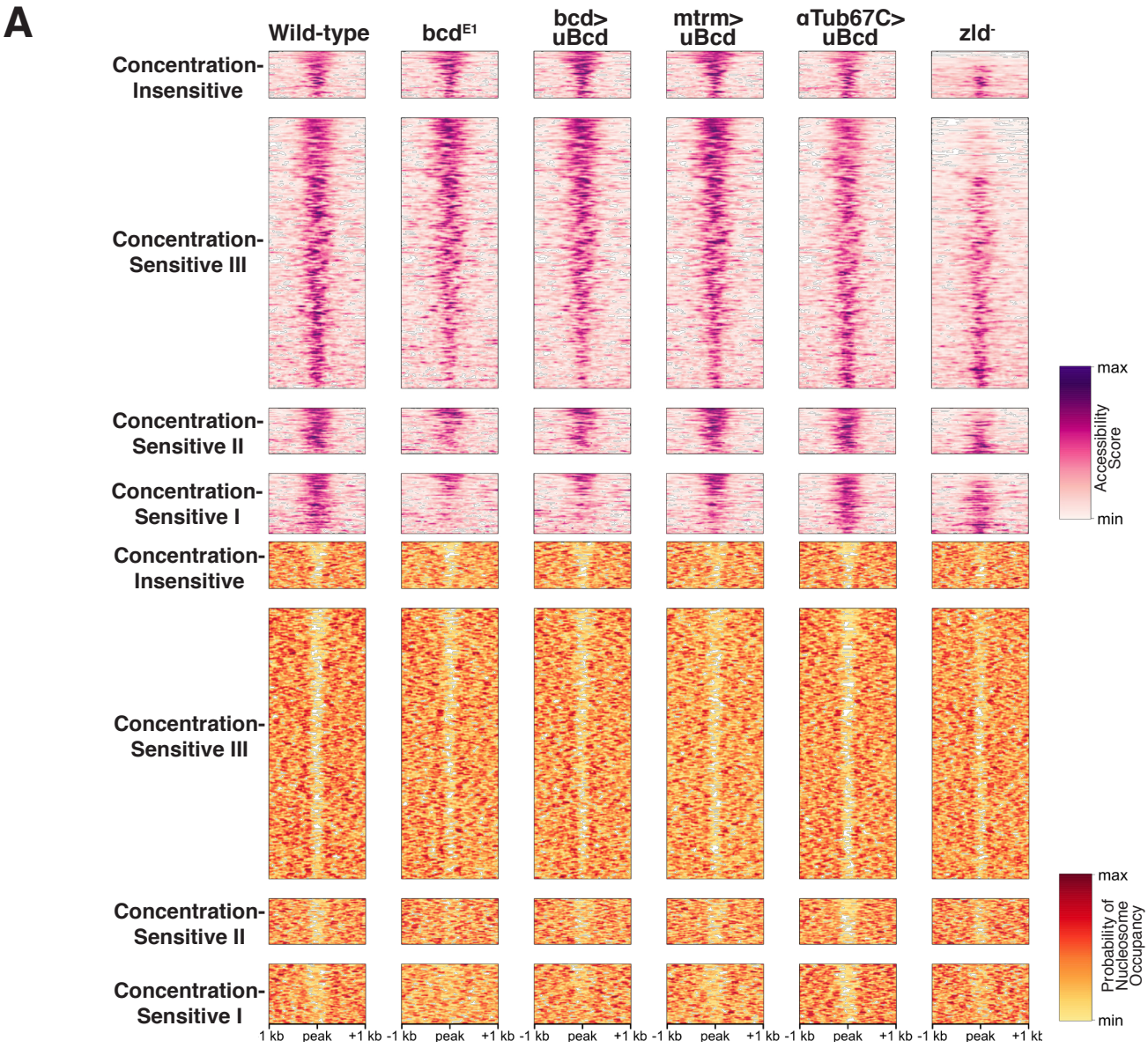

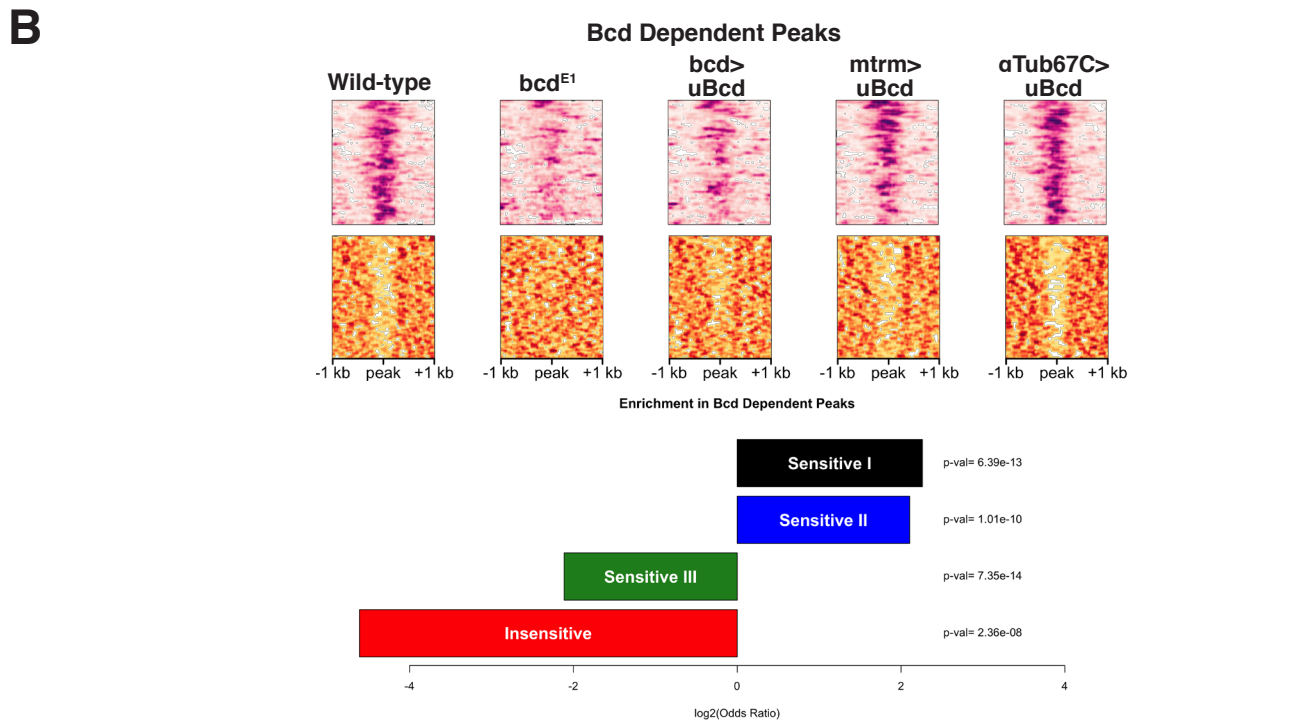

Figure 3. Bcd drives chromatin accessibility primarily at concentration-sensitive targets.

(A) Heatmaps showing chromatin accessibility (top) and probability of nucleosome occupancy (bottom) around Bcd-bound peaks from ATAC-seq experiments. Peak regions are arranged by decreasing accessibility in wild-type embryos. *bcd*^{E1} mutant embryos show a loss of accessibility and increased nucleosome occupancy most strongly at the Concentration-Sensitive I and II peaks. *zld*$^{-}$ embryos show reduced accessibility across all sensitivity classes.

(B) Subset of 132 Bcd-bound peaks selected from (A) that become inaccessible in the absence of Bcd. Accessibility at these peaks increases with increasing concentrations of uniform Bcd. Odds ratios and p-values calculated from Fisher's exact test show significant overrepresentation of the Concentration-Sensitive I and II classes in the Bcd-dependent peaks.

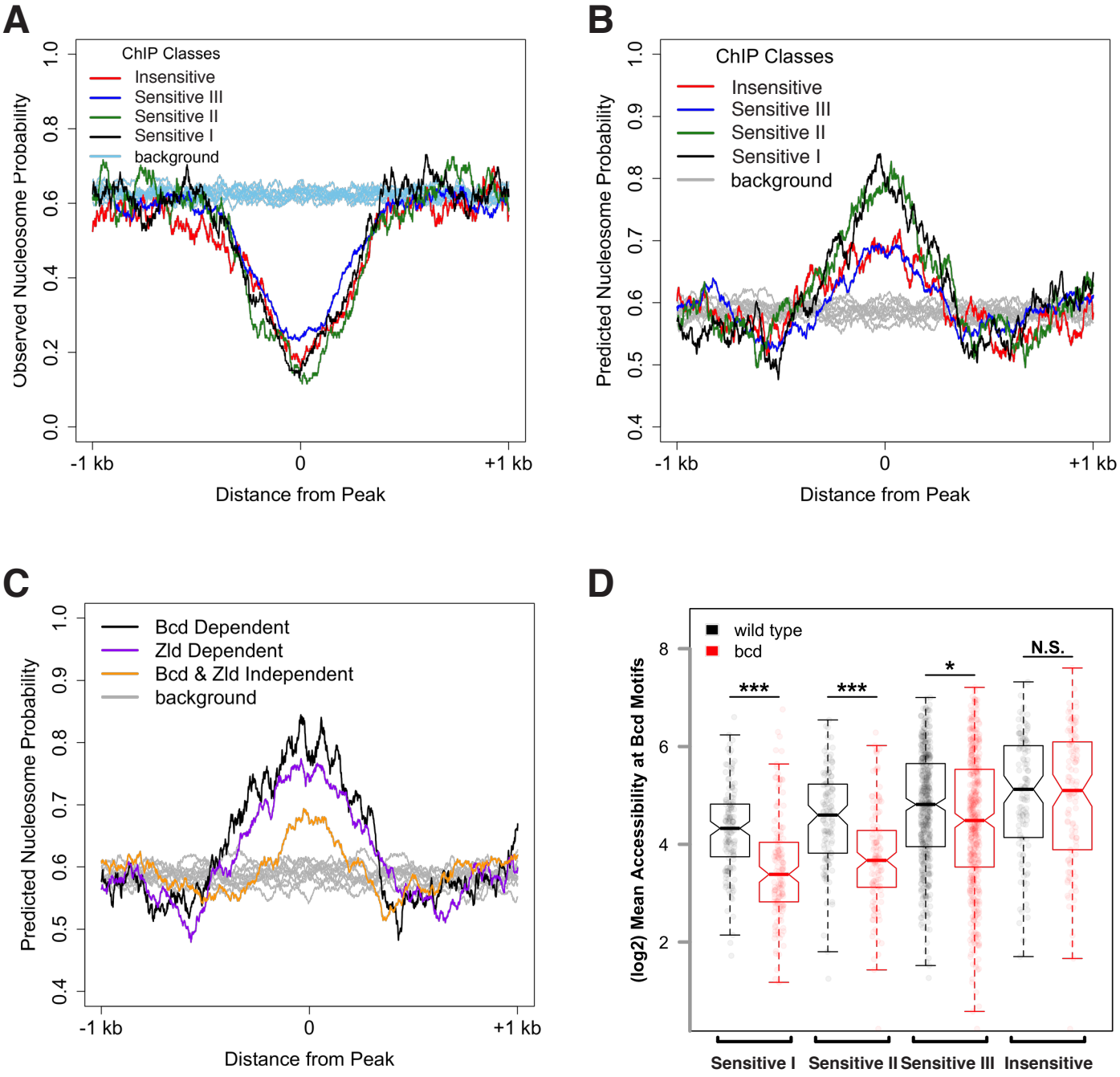

Figure 4. Bcd sensitivity classes differ in both predicted and observed nucleosome occupancy.

(A) Metaprofiles of nucleosome occupancy in each sensitivity class in wild-type embryos. Background represents random selection of regions outside of Bcd peaks shows a genome-wide average nucleosome probability of ~0.6. Bcd-bound peak regions show reduced nucleosome occupancy compared to unbound regions.

(B) Predicted nucleosome occupancy using NuPoP show higher modeled probability of nucleosome occupancy in Bcd-bound peaks relative to background regions, with higher probability of occupancy at the Concentration-Sensitive I and II classes.

(C) Predicted nucleosome occupancy in peaks dependent on Bcd vs. Zld (n_{Bcd}=132 peaks, n_{Zld}=402 peaks, with n=61 peaks dependent on both Bcd and Zld) for accessibility show higher predicted occupancy than peaks independent of both Bcd and Zld (n=554).

(D) Mean wild type (black) or *bcd*$^{-}$ (red) ATAC accessibility scores for Bcd motifs were calculated for each peak and plotted by sensitivity group. Boxplots depict the distribution of accessibility scores for each group in each genotype, and individual data points are shown as points. P-values were calculated by one-sided permutation test and indicate the likelihood in a randomly selected population of observing a difference between means greater than the observed values ($p < 1e-6$ for Concentration-Sensitive I and II groups, $p = 0.001207$ for Concentration-Sensitive III, and $p = 0.988167$ for Concentration-Insensitive).

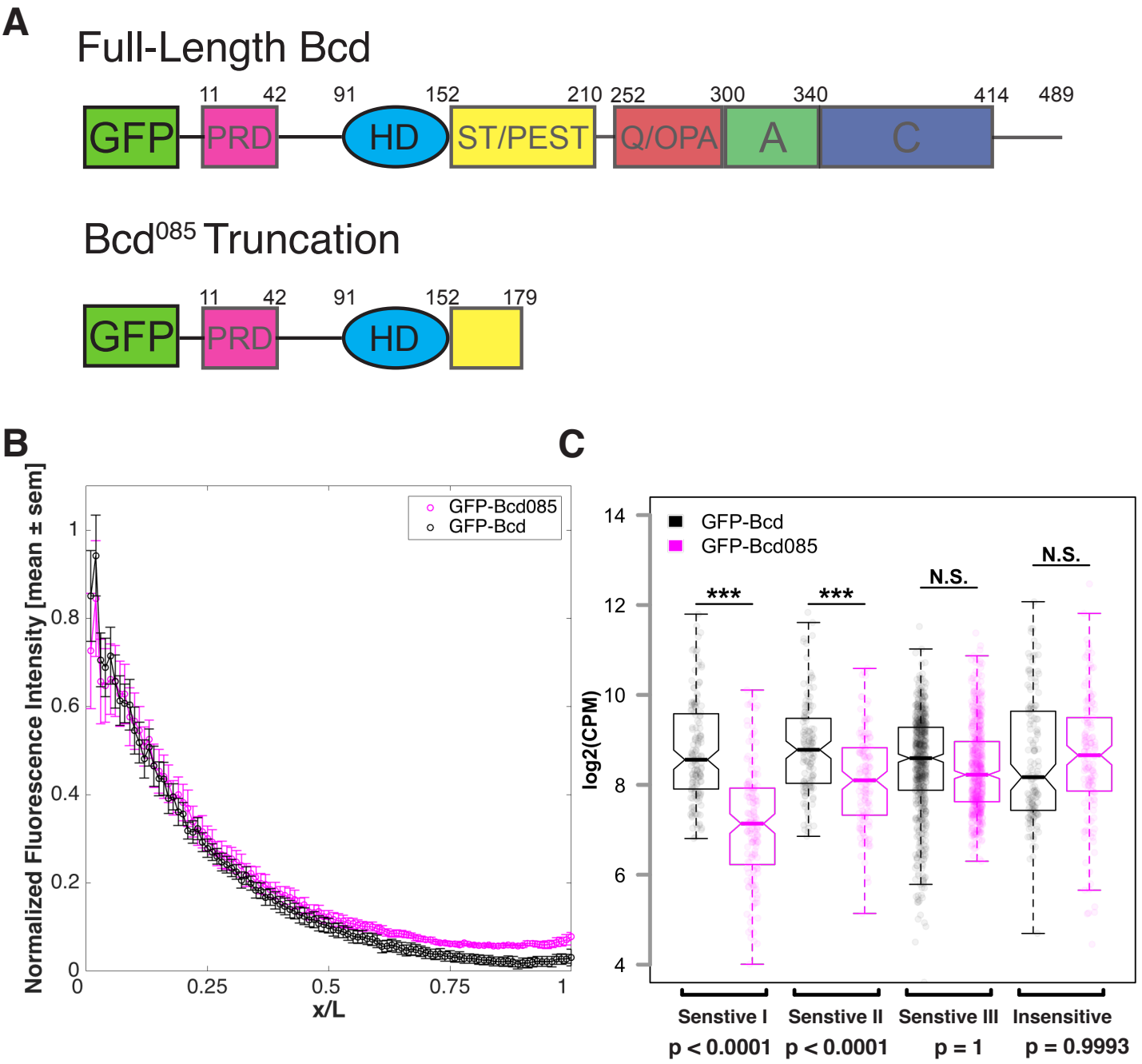

Figure 5. Bicoid requires C-terminal protein domains to bind to concentration-sensitive targets.

(A) GFP-Bcd^{085} construct is truncated within the S/T domain downstream of the homedomain. Wild-type protein domains modified from (Janody et al., 2001) and (Crauk and Dostatni, 2005) . The N-terminus of the protein includes a PRD repeat, followed by the DNA-binding homeodomain (HD) (Berleth et al., 1988). The serine/threonine-rich (S/T) domain is the target of MAPK phosphorylation by the terminal patterning Torso pathway (Janody et al., 2000) and contains a PEST sequence implicated in targeting the protein for degradation (Rechsteiner and Rogers, 1996). The C-terminus contains three domains implicated in transcriptional activation. The glutamine-rich (Q)/OPA and alanine-rich (A) domains are required for interactions with TAFII110 and TAFII60, respectively (Sauer et al., 1995). The acidic (C) domain has been demonstrated to play a role in transcriptional activation in yeast, but is not required for Bicoid activity in the embryo (Driever et al., 1989a).

(B) GFP-Bcd^{085} forms a protein gradient comparable to wild-type GFP-Bcd. GFP fluorescence intensity was extracted from dorsal profiles of live embryos. Error bars are standard error of the mean: GFP-Bcd embryos, n = 8; and GFP-Bcd^{085} embryos, n = 8.

(C) Boxplots displaying log transformed CPM normalized ChIP-seq data from GFP-Bcd;;bcd^{E1} (wild-type) and GFP-Bcd^{085};bcd^{E1} (Bcd^{085}) embryos show significant reduction binding of Bcd^{085} in Concentration-Sensitive I and II peaks. P-values were calculated from permutation tests (n = 10,000). See also Figure 2 Figure Supplement 2.

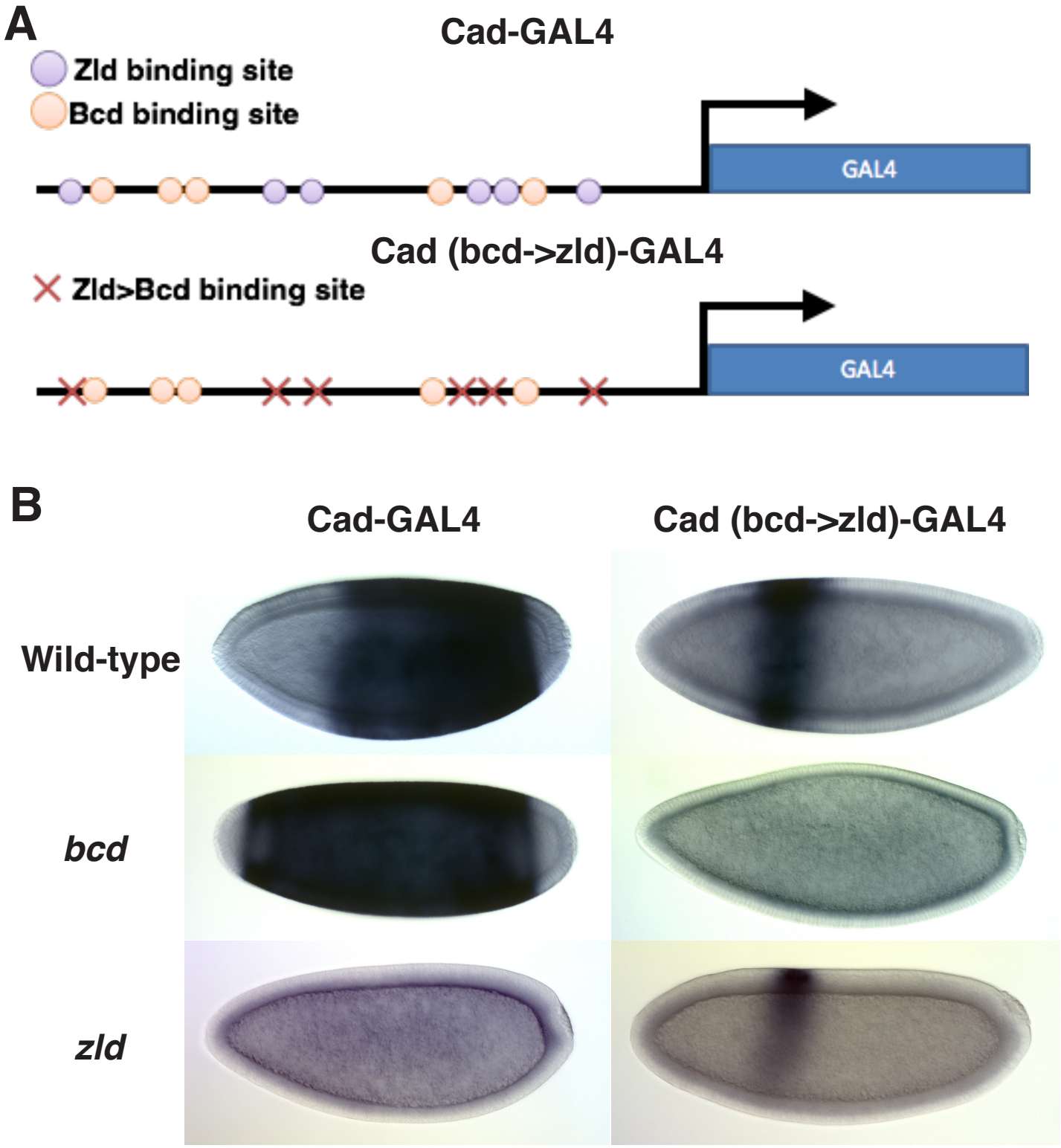

Figure 6. Replacing Zld sites with Bcd sites shifts gene expression to the anterior.

(A) Schematic of the Vienna Tile enhancer reporter for *caudal*, containing 5 Zld and 6 Bcd binding sites. The mutated reporter contains 11 Bcd binding sites and no Zld sites.

(B) Expression of the wild-type and mutated reporter in wild-type, *bcd*$^{-}$or *zld*$^{-}$ embryos.

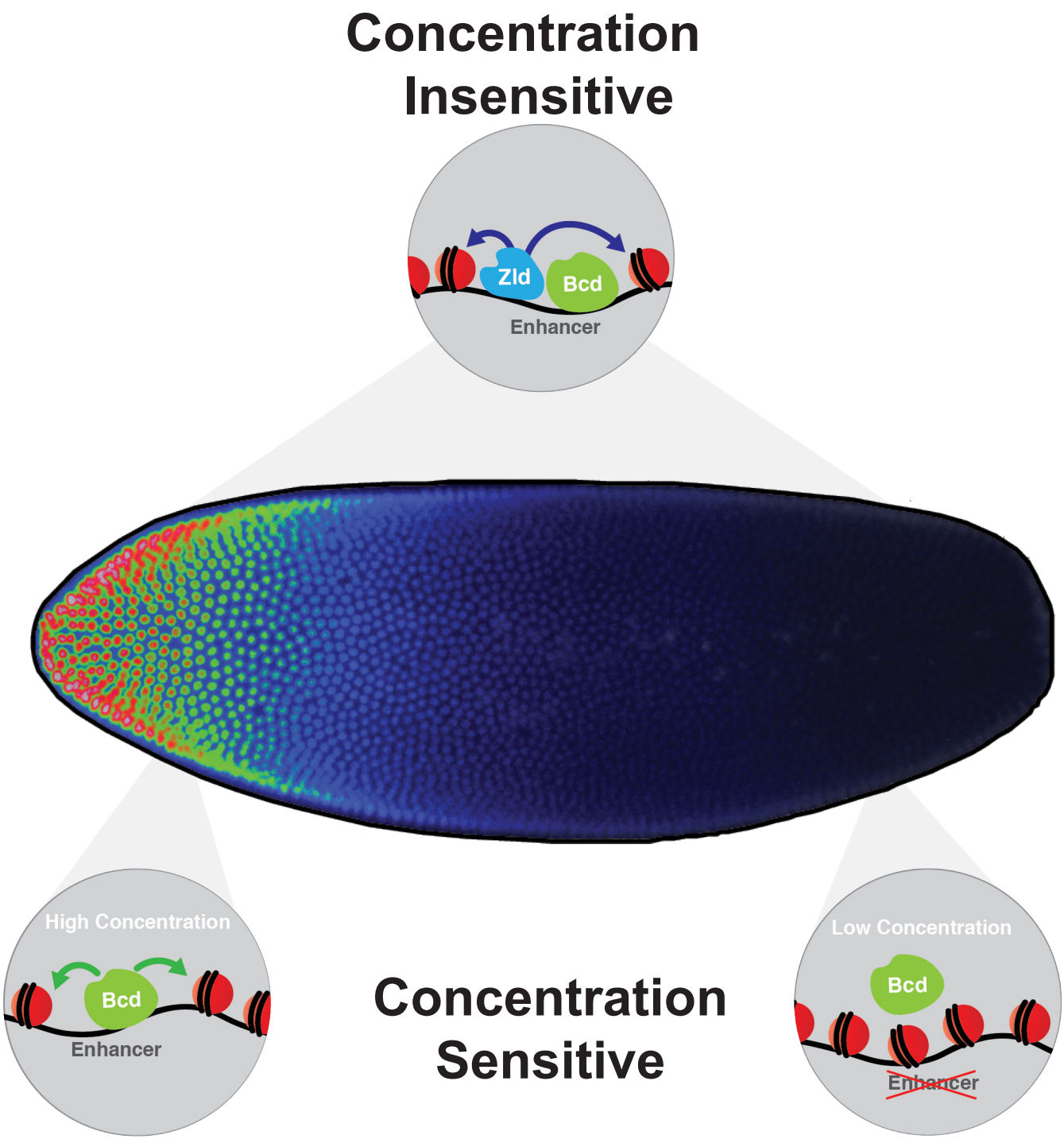

Figure 7. Model for Bicoid function along the AP axis.

Bcd drives accessibility of concentration-sensitive, Bcd-dependent enhancers at high concentrations in anterior nuclei, and these sites are closed in posterior nuclei. concentration-insensitive targets remain accessible in both anterior and posterior nuclei, likely through inputs from other factors such as Zld and more open local chromatin structure with a lower nucleosome preference.

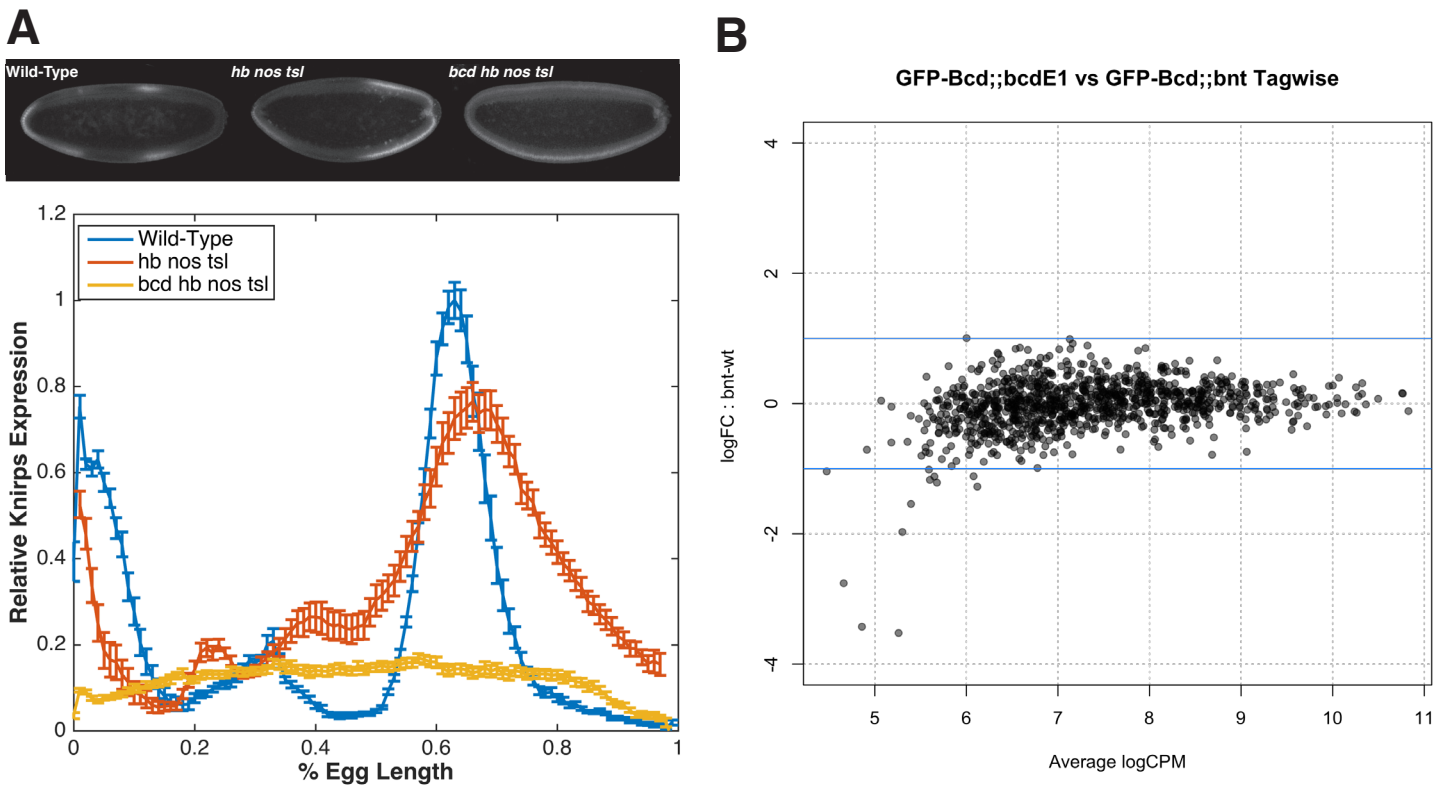

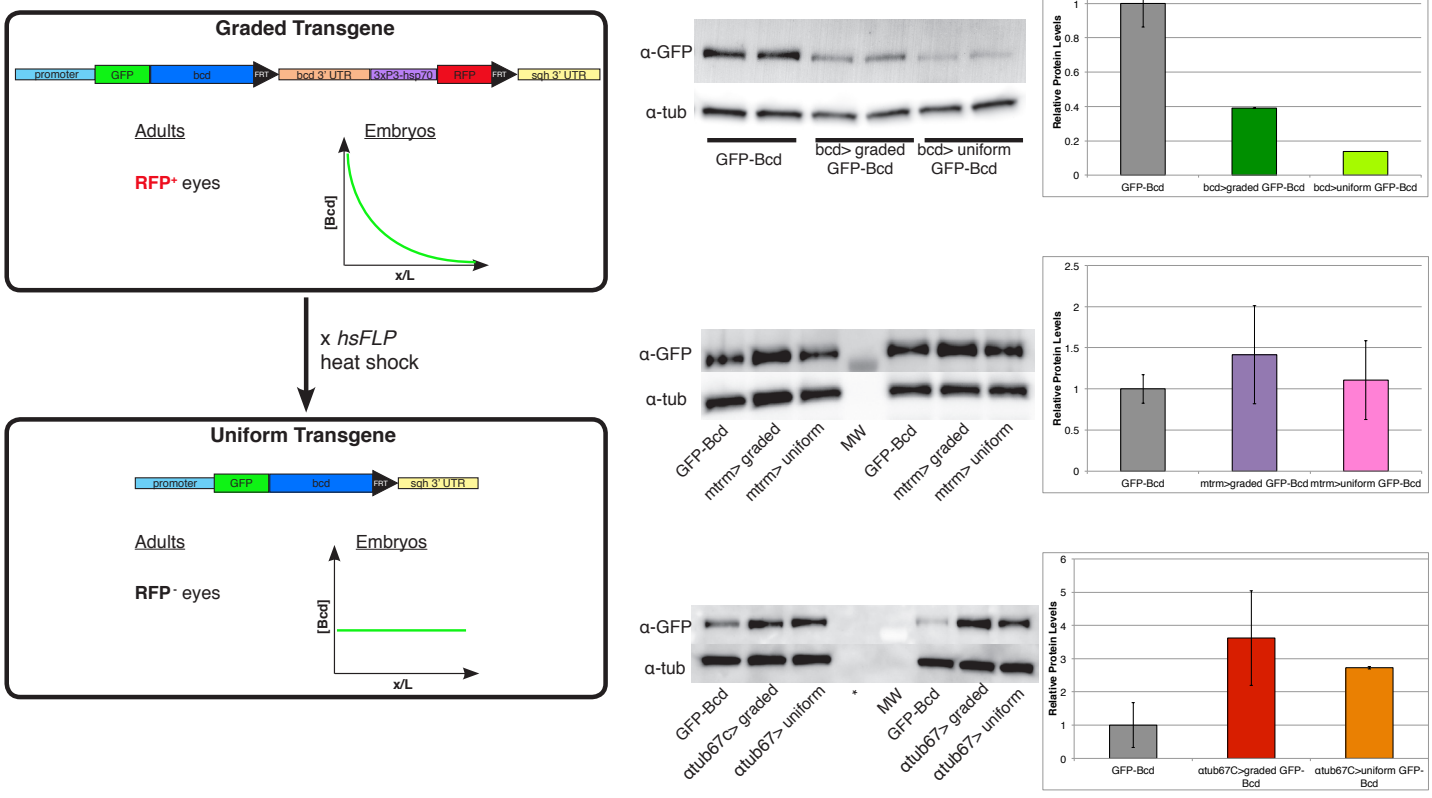

Figure 1 Figure Supplement 1.

A) Quanitification of Knirps intensity in wild-type, triple mutant (*hb nos tsl*) and quadruple mutant (*bcd hb nos tsl*). Bicoid activates patterned expression of Knirps. In embryos in which Bicoid is the only source of maternal patterning information (*hb nos tsl*), a broad domain of Kni is expressed in the posterior of the embryo. In quadruple mutant embryos, a low level of uniform Knirps is expressed ubiquitously, suggesting that Bcd is required for activating expression of *knirps* above a background level. Heat-fixed embryos from wild-type (Oregon-R) mothers, *hunchback nanos torso-like* germline clones and *bicoid hunchback nanos torso-like* germline clones were pooled and immunostained in a single tube with a rat anti-Knirps primary antibody and Alexa-647 rat antibody. Embryos were mounted on a single slide and imaged by confocal microscopy. Representative embryos for each genotype are shown. Fluorescence intensity of Knirps was extracted from dorsal profiles of midsagittal sections of embryos and plotted using MATLAB. Data are fluorescence intensity minus background, and error bars are standard error of the mean for n = 5 wild-type, n = 8 *hb nos tsl,* and n = 6 *bcd hb nos tsl* embryos.

B) Smear plot generated in EdgeR (Robinson et al., 2010) showing the log transformed fold-change in Bcd binding between mutant and wild-type embryos for each Bcd peak, vs. the average log transformed sequencing read counts per million (CPM). Bcd binding shows no significant changes between wild-type and *nos tsl* mutant embryos. Significance was determined using EdgeR to perform a pairwise exact test with a cutoff of FDR ≤ 0.05, comparing binding between *eGFP-Bcd;;bcd*^{E1} and *eGFP-Bcd;; bcd*^{E1} *hb*^{FB} *nos*^{L7} *tsl*^{4} in the 1,027 Bcd peaks.

C) Schematic of the uniform Bcd transgene. The uniform Bcd transgene contains an N-terminal GFP-tagged Bcd driven by the various maternal promoters discussed in the text. Downstream of the *bcd* coding sequence is a cassette containing the endogenous *bcd* 3'UTR and a 3xP3-hsp70 promoter driving promoter of RFP. This cassette is flanked by FRT sites. The *sqh* 3'UTR lies downstream of the FRT cassette. Flies expressing this version of the transgene can be identified by RFP expression in their eyes, and females produce embryos in which Bcd is distributed in a gradient.
Males from this transgenic stock are crossed to females expressing a heat shock inducible flippase (*hsFLP)*, and heat shocking the F1 larvae results in recombination and excision of the cassette at the FRT sites, bringing the *sqh* 3'UTR directly downstream of the *bcd* coding sequence. This initially results in mosaic F1 flies with a mosaic graded/uniform Bcd germline. The F1 are further outcrossed to bcd^{E1} mutants and F2 individuals producing embryos with uniform Bcd distributions can be identified by the lack of RFP expression in the eyes.
D) Expression levels of uniform Bcd constructs measured by western blots.
Western blots for GFP-Bcd were performed on embryos at NC14. Representative gels and quantifications are shown for the bcd promoter-driven transgene (A), mtrm promoter-driven transgene (B) and α-tub67C promoter-driven transgene (C). In the barplots, band intensities are reported relative to wild-type (GFP-Bcd). All lanes are normalized to an α-tubulin loading control. Error bars are standard deviation between two biological replicates for each sample. MW = molecular weight marker, * = skipped lane.

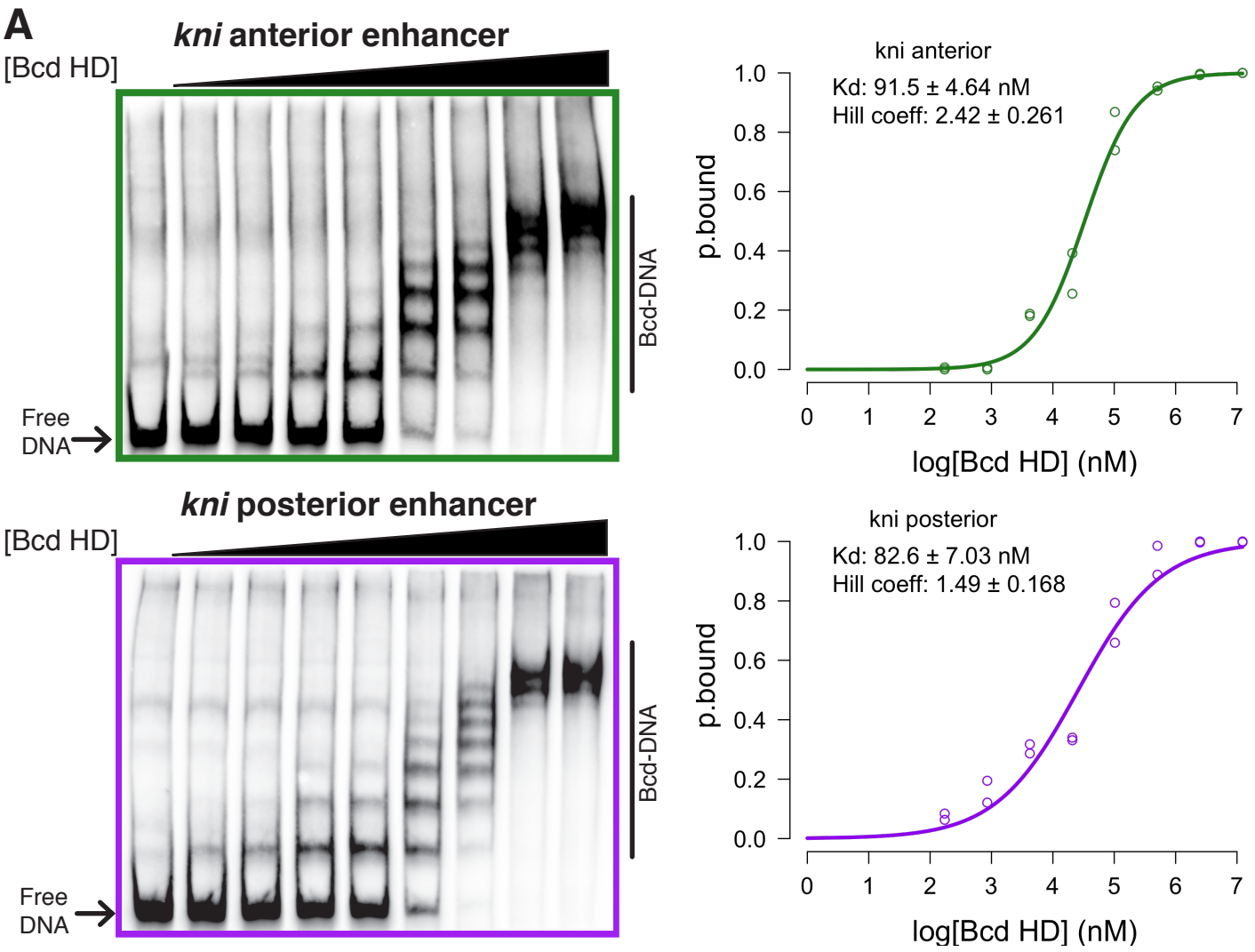

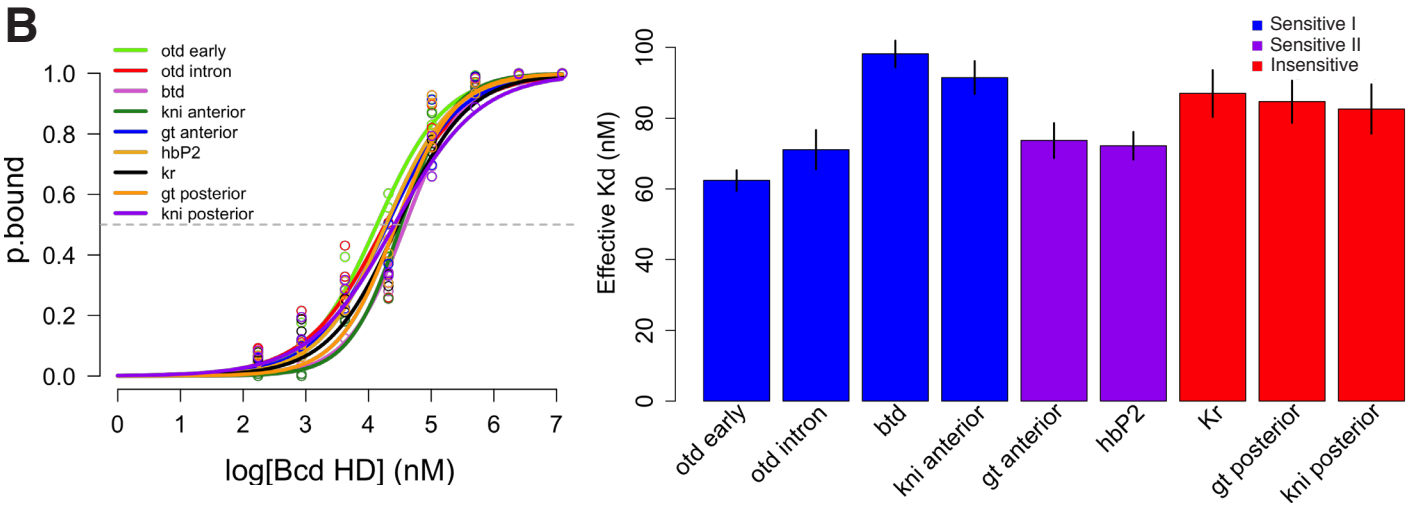

Figure 2 Figure Supplement 1. *In vitro* binding affinity of target enhancers for Bcd protein is insufficient to explain *in vivo* binding behavior.

(A) Representative gels from EMSAs with *kni* anterior or posterior enhancer sequence used as DNA probe. Binding curves display the log transformed Bcd concentration is plotted vs. ratio of bound to shifted probe (p.bound).

(B) Binding curves for nine EMSA probes show largely overlapping profiles of *in vitro* affinity for Bcd.

(C) Effective K_d measurements for nine EMSA probes do not correspond to *in vivo* behavior of the same DNA sequences. *In vivo* sensitivity classifications determined by ChIP-seq are indicated by color of bars. Error bars are standard error from 2-3 technical replicates per DNA probe.

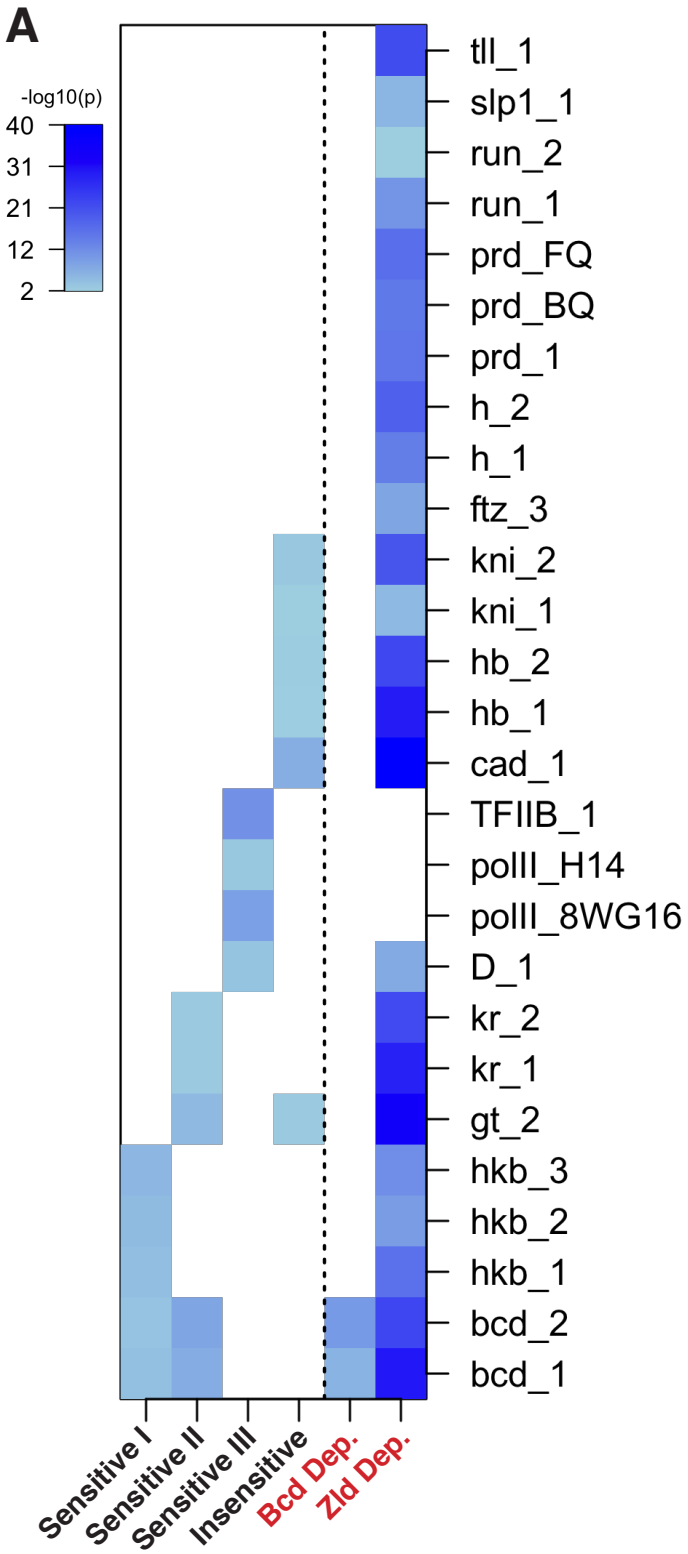

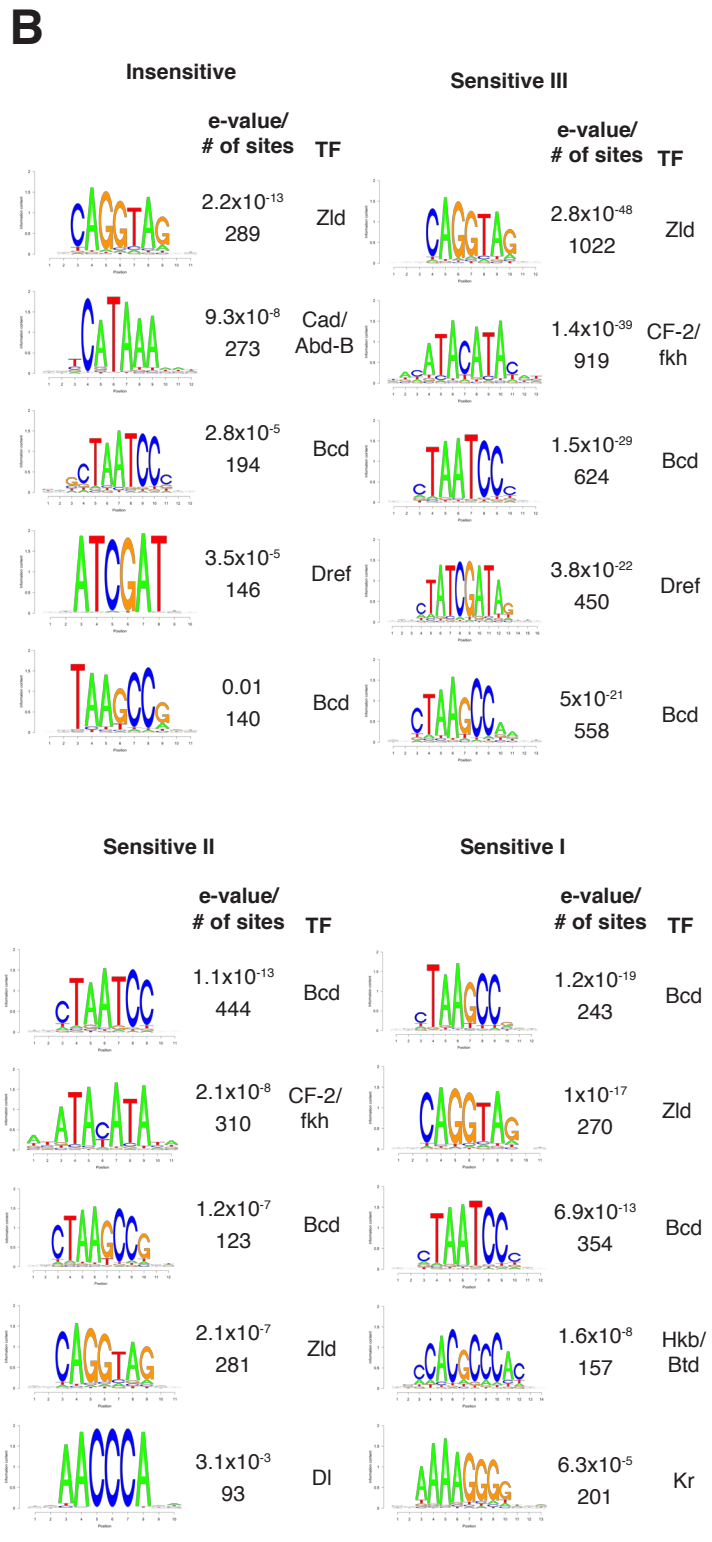

Figure 2 Figure Supplement 2. Enrichment for binding and motifs of transcription factors in Bcd sensitivity classes.

(A) Heatmap depicting enrichment of Berkeley Drosophila Transcription Network Project (BDTNP) ChIP-chip peaks for AP factors in Bcd-bound sensitivity classes. ChIP data (MacArthur et al., 2009) was downloaded from bdtnp.lbl.gov, and overlap between ChIP peaks for the indicated factors/antibodies and either the Bcd sensitivity classes or ATAC-seq accessibility dependence groups were calculated. One-sided Fisher's exact tests were performed to test for enrichment of a BDTNP ChIP peak set within given Bcd peak class. P-values are plotted as -log10 values, where white indicates non-significant values.

(B) *De novo* motif discovery performed with RSAT as in Figure 2B, for each of the Bcd sensitivity classes individually. The top five enriched motifs are displayed for each sensitivity class.